Multi-taper S-transform method for estimating Wigner-Ville and Loève spectra of quasi-stationary harmonizable processes

Zifeng Huang[a,*], Guan Chen[a], Michael Beer[a, b, c]

[a]*Institute for Risk and Reliability, Leibniz Universiy Hannover, Callinstr. 34, Hannover 30167, Germany*

[b]*Institute for Risk and Uncertainty, University of Liverpool, Peach Street, Liverpool L69 7ZF, United Kingdom*

[c]*International Joint Research Center for Resilient Infrastructure & International Joint Research Center for Engineering Reliability and Stochastic Mechanics, Tongji University, Shanghai 200092, PR China*

Abstract: Current non-stationary load models based on the evolutionary power spectral density (EPSD) may lead to overestimation and ambiguity of structural responses. The quasi-stationary harmonizable process with its Wigner-Ville spectrum (WVS) and Loève spectrum, which do not suffer from the deficiencies of EPSD, is suitable for modeling non-stationary loads and analyzing their induced structural responses. In this study, the multi-taper S-transform (MTST) method for estimating WVS and Loève spectrum of multi-variate quasi-stationary harmonizable processes is presented. The analytical biases and variances of the WVS, Loève spectrum, and time-invariant and time-varying coherence estimators from the MTST method are provided under the assumption that the target multi-variate harmonizable process is Gaussian. Using a numerical case of a bivariate harmonizable wind speed process, the superiority and reliability of the MTST method are demonstrated through comparisons with several existing methods for the WVS and Loève spectrum estimations. Finally, the MTST method is applied to two pieces of ground motion acceleration records measured during the Turkey earthquake in 2023.

Keywords: MTST method; Harmonizable process; Wigner-Ville spectrum; Loève spectrum; Time-varying coherence.

*Corresponding author

Email address: zifeng.huang@irz.uni-hannover.de (Zifeng Huang), guan.chen@irz.uni-hannover.de (Guan Chen), beer@irz.uni-hannover.de (Michael Beer)

1. Introduction

Random environmental loads, such as extreme wind events (tropical storm and downburst) and earthquake ground motion, are usually non-stationary. Owing to the preservation of physical interpretation of local power-frequency distribution at each time instant, the evolutionary power spectral density (EPSD) [1, 2] has wide application in the characterization and simulation of non-stationary earthquake ground motions [3-5] and non-stationary wind speeds [6-9], and the prediction of structural responses [7, 10-13]. Though being popular, EPSD has two essential deficiencies. First, it is difficult to calculate an accurate structural response EPSD directly from the load EPSD through the structural frequency response function. The quasi-stationary approximation [14], which assumes that the load EPSD is slowly-varying, provides an approximate frequency domain calculation. However, for transient loads, this approximation may overestimate the structural responses caused by downbursts [7] and is in general invalid for the structural responses caused by earthquake ground motions [14]. Second and more significant, for a multi-variate non-stationary load with time-varying coherences, its correlation is calculated by decomposing its EPSD matrix. When different decomposition methods, e.g., Cholesky decomposition [3] or proper orthogonal decomposition [15], are used, the obtained correlation may be not unique [16].

The harmonizable process [17, 18] is a direct extension of the wide-sense stationary process by considering the spectral correlation. For a harmonizable process, its Wigner-Ville spectrum (WVS) represents the time-frequency properties and its Loève spectrum, a dual-frequency spectrum, characterizes the spectral correlation. The WVS, Loève spectrum, and correlation function of a harmonizable process are in one-to-one correspondence and can be converted to each other by one-dimensional (1D) or two-dimensional (2D) Fourier transform [19, 20]. Given a linear-elastic structure subjected to a harmonizable load, the Loève spectrum of the structural response can be directly calculated by multiplying the load Loève spectrum by the structural frequency response function [21]. In addition, similar to the semi-stationary process characterized by a slowly-varying ESPD [1], a quasi-stationary harmonizable process with a non-negative slowly-varying WVS [22] could characterize the time-frequency properties of non-stationary loads. Thus, the quasi-stationary harmonizable process with its WVS and Loève spectrum is suitable for modeling non-stationary loads and analyzing their induced structural responses.

For modeling harmonizable loads, accurately estimating the WVS and Loève spectrum of the loads using field-measured data is a fundamental and challenging issue. For the WVS estimation of harmonizable processes, a general class of estimators is in the form of a time-varying Fourier transform with various time-domain kernels [20, 22-25]. These kernels include those formed by single time windows corresponding to the spectrogram [22]; those formed by the separable time-frequency windows corresponding to the pseudo-Wigner estimator [22]; those formed by a weighted sum of the kernels for the spectrogram or by a weighted sum of the kernels for the pseudo-Wigner estimator [26]; those formed by multi-tapers [27, 28]; and Toeplitz and Hankel kernels [29].

For the Loève spectrum estimation, a general class of estimators is in the form of a 2D Fourier transform of various tapered correlation estimators [30]. These Loève spectrum estimators include the biperiodgram, which is a tensor product of a tapered Fourier transform [31]; the temporally or spectrally smoothed biperiodgram [32-34]; and the multi-taper estimator [35, 36]. A comprehensive review of these estimators for the cyclostationary signals is given by Antoni [30]. Another class of Loève spectrum estimators is formed by performing a 1D Fourier transform on several WVS estimators. This class includes that calculated from the WVS estimator using Toeplitz kernels [37] and the cyclic modulation spectrum (CMS) calculated from the spectrogram [38, 39].

Utilizing constant kernels, the time-frequency resolution capabilities of the WVS estimators mentioned above remain fixed all over the time-frequency domain. However, the time-frequency spectra of non-stationary loads, varying obviously over the time-frequency domain, need different time-frequency resolutions at different time-frequency points. These WVS estimators cannot satisfy this requirement. Similar to the wavelet transform, the affine WVS [40-42], including its multi-taper version [27], could provide scale-dependent resolutions in the time-scale domain but not directly in the time-frequency domain. Most of the Loève spectrum estimators based on the 2D Fourier transform, and the cyclic modulation spectrum were developed for the spectrally correlated processes whose Loève spectra consist of a countable set of lines or curves in the dual-frequency plane [33]. However, environmental non-stationary loads usually have a Loève spectrum, which is a continuous surface concentrated near the main diagonal line of the dual-frequency plane, e.g., the Loève spectrum of an earthquake ground motion acceleration [43]. The Loève spectrum estimation of non-stationary loads needs both a large frequency resolution and a low estimation variance, which the Loève spectrum estimators mentioned above are difficult to satisfy. The Loève spectrum estimator from the WVS estimator using Toeplitz kernels was merely proposed in [37] without any further study about its mathematical properties or applicability to various kinds of stochastic processes.

The multi-taper S-transform (MTST) [44-46], which is a spectrogram with a set of orthogonal time-frequency windows, could form a multi-taper affine WVS estimator with frequency-dependent resolutions in the time-frequency domain. Thus, the MTST is suitable for the WVS estimation of non-stationary loads. In this study, the MTST method for the WVS and Loève spectrum estimations of quasi-stationary harmonizable processes is proposed. Specifically, a WVS estimator from the MTST, a Loève spectrum estimator from the MTST-based WVS estimator, and time-invariant and time-varying coherence estimators are given. The biases and variances of these estimators are provided under the assumption that the target multi-variate harmonizable process is Gaussian.

The remainder of this paper is organized as follows. First, the mathematical definition, spectral properties, and the quasi-stationary condition of harmonizable processes are introduced. Subsequently, the mathematical foundation of the MTST method for the WVS and Loève spectrum estimations is established. Next, using a numerical case of a bivariate harmonizable wind speed process, the superiority and reliability of the MTST method, especially its feasibility for one realization, are confirmed through comparisons with several existing methods. Finally, the MTST method is applied to two pieces of ground motion acceleration records measured during the Turkey earthquake in 2023.

In this study, $\mathbb{R}$ denotes the set of real numbers, $\mathbb{Z}$ denotes the set of integers, and $\mathbb{Z}^+$ denotes the set of positive integers. In the dual-frequency plane whose coordinate is (f_1, f_2), the main diagonal line is referred as the line of $f_1 = f_2$. Since the field-measured data of real environmental loads are finite-length discrete-time records, discrete-time computation is considered in the Fourier transforms in this study.

2. Harmonizable process

A zero-mean, second-order, and real-valued multi-variate harmonizable process $\mathbf{X}(t) = [X_1(t),$

$X_2(t)$,…, $X_N(t)]^{\mathrm{T}}$ is defined as [18]

$$\mathbf{X}(t) = \int_{-f_{\mathrm{N}}}^{f_{\mathrm{N}}} e^{\mathrm{i}2\pi ft} \mathrm{d}\mathbf{Z}(f), \tag{1}$$

where T is the transposition operator, $t = k\Delta t$, $k \in \mathbb{Z}$, Δt is the sample interval, $f_{\mathrm{s}} = 1/\Delta t$ is the sampling frequency, $f_{\mathrm{N}} = f_{\mathrm{s}}/2$ is the Nyquist frequency, $\mathbf{Z}(f) = [Z_1(f),\ Z_2(f)\ ,…,\ Z_N(f)]^{\mathrm{T}}$ is a complex-valued zero-mean process satisfying

$$\mathrm{d}\mathbf{Z}^*(f) = \mathrm{d}\mathbf{Z}(-f), \tag{2}$$

and $*$ is the conjugate operator. In this study, $\mathbf{Z}(f)$ is assumed to be zero outside the range of $[-f_{\mathrm{N}},\ f_{\mathrm{N}}]$. Thus, the integration interval in Eq. (1) can be extended to $(-\infty, +\infty)$.

The Loève spectrum of $\mathbf{X}(t)$ is defined as [17, 47]

$$\mathbf{S}(f_1, f_2) = \mathrm{E}\left[\mathrm{d}\mathbf{Z}^*(f_1)\mathrm{d}\mathbf{Z}^{\mathrm{T}}(f_2)\right] \big/ \mathrm{d}f_1 \mathrm{d}f_2\,, \tag{3}$$

where E is the expectation operator. $\mathbf{S}(f_1,\ f_2)$ satisfies

$$\mathbf{S}^*(f_1, f_2) = \mathbf{S}^{\mathrm{T}}(f_2, f_1). \tag{4}$$

The correlation $\mathbf{R}(t_1,\ t_2) = \mathrm{E}[\mathbf{X}^*(t_1)\mathbf{X}^{\mathrm{T}}(t_2)]$ of $\mathbf{X}(t)$ is calculated as

$$\mathbf{R}(t_1, t_2) = \int_{-\infty}^{+\infty}\int_{-\infty}^{+\infty} e^{\mathrm{i}2\pi(f_2 t_2 - f_1 t_1)} \mathrm{E}\left[\mathrm{d}\mathbf{Z}^*(f_1)\mathrm{d}\mathbf{Z}^{\mathrm{T}}(f_2)\right] = \int_{-\infty}^{+\infty}\int_{-\infty}^{+\infty} e^{\mathrm{i}2\pi(f_2 t_2 - f_1 t_1)} \mathbf{S}(f_1, f_2)\mathrm{d}f_1 \mathrm{d}f_2. \tag{5}$$

Since $\mathbf{S}(f_1,\ f_2)$ is zero outside the range of $[-f_{\mathrm{N}},\ f_{\mathrm{N}}]^2$, $\mathbf{S}(f_1,\ f_2)$ and $\mathbf{R}(t_1,\ t_2)$ are assumed to constitute a 2D Fourier transform pair, as indicated in Eq. (5) and the following one

$$\mathbf{S}(f_1, f_2) = \Delta t^2 \sum_{k=-\infty}^{+\infty}\sum_{l=-\infty}^{+\infty} e^{\mathrm{i}2\pi(f_1 k\Delta t - f_2 l\Delta t)} \mathbf{R}(k\Delta t, l\Delta t), \tag{6}$$

where f_1 and $f_2 \in [-f_{\mathrm{N}},\ f_{\mathrm{N}}]$.

Rotating the time coordinate in $\mathbf{R}(t_1,\ t_2)$ and the frequency coordinate in $\mathbf{S}(f_1,\ f_2)$ by 45°, respectively, that is $t = 0.5(t_1 + t_2)$ and $\tau = (t_2 - t_1)$, $f = 0.5(f_1 + f_2)$ and $\xi = (f_2 - f_1)$, $\widetilde{\mathbf{R}}(t,\ \tau) = \mathbf{R}(t - 0.5\tau,\ t + 0.5\tau)$ and $\tilde{\mathbf{S}}(f,\ \xi) = \mathbf{S}(f - 0.5\xi,\ f + 0.5\xi)$ are obtained. $\widetilde{\mathbf{R}}(t,\ \tau)$ can be calculated as

$$
\begin{aligned}
&\tilde{\mathbf{R}}(t,\tau)\\
&=\int_{-f_\mathrm{N}}^{f_\mathrm{N}}\int_{-f_\mathrm{N}}^{f_\mathrm{N}} e^{\mathrm{i}2\pi[f_2(t+0.5\tau)-f_1(t-0.5\tau)]}\mathbf{S}(f_1,f_2)\mathrm{d}f_1\mathrm{d}f_2\\
&=\int_{-f_\mathrm{N}}^{0}\int_{-2f_\mathrm{N}-2f}^{2f_\mathrm{N}+2f} e^{\mathrm{i}2\pi[(f+0.5\xi)(t+0.5\tau)-(f-0.5\xi)(t-0.5\tau)]}\mathbf{S}[(f-0.5\xi),(f+0.5\xi)]\mathrm{d}\xi\mathrm{d}f\\
&\quad+\int_{0}^{f_\mathrm{N}}\int_{-2f_\mathrm{N}+2f}^{2f_\mathrm{N}-2f} e^{\mathrm{i}2\pi[(f+0.5\xi)(t+0.5\tau)-(f-0.5\xi)(t-0.5\tau)]}\mathbf{S}[(f-0.5\xi),(f+0.5\xi)]\mathrm{d}\xi\mathrm{d}f\\
&=\int_{-f_\mathrm{N}}^{0}\int_{-2f_\mathrm{N}-2f}^{2f_\mathrm{N}+2f} e^{\mathrm{i}2\pi(f\tau+\xi t)}\tilde{\mathbf{S}}(f,\xi)\mathrm{d}\xi\mathrm{d}f+\int_{0}^{f_\mathrm{N}}\int_{-2f_\mathrm{N}+2f}^{2f_\mathrm{N}-2f} e^{\mathrm{i}2\pi(f\tau+\xi t)}\tilde{\mathbf{S}}(f,\xi)\mathrm{d}\xi\mathrm{d}f\\
&\overset{(a)}{=}\int_{-f_\mathrm{N}}^{f_\mathrm{N}}\int_{-2f_\mathrm{N}}^{2f_\mathrm{N}} e^{\mathrm{i}2\pi(f\tau+\xi t)}\tilde{\mathbf{S}}(f,\xi)\mathrm{d}\xi\mathrm{d}f\\
&\overset{(b)}{=}\int_{-\infty}^{+\infty}\int_{-\infty}^{+\infty} e^{\mathrm{i}2\pi(f\tau+\xi t)}\tilde{\mathbf{S}}(f,\xi)\mathrm{d}\xi\mathrm{d}f,
\end{aligned}
\tag{7}
$$

where (a) and (b) is valid because $\mathbf{S}(f_1, f_2)$ only has values in the range of $(f_1, f_2) \in [-f_\mathrm{N}, f_\mathrm{N}]^2$. Then, it is obtained

$$
\tilde{\mathbf{S}}(f,\xi)=\frac{\Delta t^2}{2}\sum_{n=-\infty}^{+\infty}\sum_{m=-\infty}^{+\infty}e^{-\mathrm{i}2\pi(fn+0.5\xi m)\Delta t}\tilde{\mathbf{R}}(0.5m\Delta t,n\Delta t),
\tag{8}
$$

where $f \in [-f_\mathrm{N}, f_\mathrm{N}]$, $\xi \in [-2f_\mathrm{N}, 2f_\mathrm{N}]$, and $m, n \in \mathbb{Z}$. Thus, $\tilde{\mathbf{R}}(t, \tau)$ and $\tilde{\mathbf{S}}(f, \xi)$ also constitute a 2D Fourier transform pair.

Since $\tilde{\mathbf{R}}(t, \tau)$ and $\tilde{\mathbf{S}}(f, \xi)$ are equivalent to $\mathbf{R}(t_1, t_2)$ and $\mathbf{S}(f_1, f_2)$, respectively, they will be interchangeably used in this study. The WVS $\mathbf{W}(t, f)$ of $\mathbf{X}(t)$ is defined by [48]

$$
\mathbf{W}(t,f)=\int_{-\infty}^{+\infty}e^{\mathrm{i}2\pi\xi t}\tilde{\mathbf{S}}(f,\xi)\mathrm{d}\xi.
\tag{9}
$$

$\mathbf{W}(t, f)$ and $\tilde{\mathbf{S}}(f, \xi)$ constitute a continuous 1D Fourier transform pair with respect to t and ξ. From Eqs. (8) and (9), $\mathbf{W}(t, f)$ can be calculated with $\tilde{\mathbf{R}}(t, \tau)$

$$
\begin{aligned}
&\mathbf{W}(t,f)\\
&=\int_{-\infty}^{+\infty}e^{\mathrm{i}2\pi\xi t}\tilde{\mathbf{S}}(f,\xi)\mathrm{d}\xi\\
&=\int_{-2f_\mathrm{N}}^{2f_\mathrm{N}}e^{\mathrm{i}2\pi\xi t}\frac{\Delta t^2}{2}\sum_{n=-\infty}^{+\infty}\sum_{m=-\infty}^{+\infty}e^{-\mathrm{i}2\pi(fn+0.5\xi m)\Delta t}\tilde{\mathbf{R}}(0.5m\Delta t,n\Delta t)\mathrm{d}\xi\\
&=\Delta t\sum_{n=-\infty}^{+\infty}e^{-\mathrm{i}2\pi fn\Delta t}\left[\frac{\Delta t}{2}\sum_{m=-\infty}^{+\infty}\int_{-2f_\mathrm{N}}^{2f_\mathrm{N}}e^{-\mathrm{i}2\pi\xi(0.5m\Delta t-t)}\mathrm{d}\xi\tilde{\mathbf{R}}(0.5m\Delta t,n\Delta t)\right]\\
&=\Delta t\sum_{n=-\infty}^{+\infty}e^{-\mathrm{i}2\pi fn\Delta t}\frac{\Delta t}{2}\sum_{m=-\infty}^{+\infty}\frac{\sin[2\pi 2f_\mathrm{N}(m\Delta t/2-t)]}{\pi(m\Delta t/2-t)}\tilde{\mathbf{R}}(0.5m\Delta t,n\Delta t)\\
&\overset{(a)}{=}\Delta t\sum_{n=-\infty}^{+\infty}e^{-\mathrm{i}2\pi fn\Delta t}\tilde{\mathbf{R}}(t,n\Delta t),
\end{aligned}
\tag{10}
$$

where (a) is from the Nyquist-Shannon sampling theorem [49].

In this study, two assumptions are enforced to $\mathbf{X}(t)$. One is that $\mathbf{X}(t)$ is assumed to be quasi-stationary, that is $\tilde{\mathbf{R}}(t, \tau)$ is slowly-varying with respect to t [22]. Specifically, given a time instant t, there exists an auto-correlation function $r_t(\tau)$ and an interval T_t for τ, in which it is satisfied [22]

$$\left|\tilde{\mathbf{R}}(t,\tau) - r_t(\tau)\right| < \varepsilon, \tag{11}$$

where $\varepsilon > 0$ is a threshold of this approximation. The minmum T_t, $T_{\min} = \min_t(T_t)$, is the time of stationarity. $\mathbf{X}(t)$ is quasi-stationary if $T_{\min} > 0$ for a given ε. $\mathbf{W}(t, f)$ of a quasi-stationary $\mathbf{X}(t)$ is also slowly-varying with respect to t. The other assumption is that the auto-WVSes of $\mathbf{X}(t)$, $W_{ii}(t, f)$ and $i = 1, 2, \ldots, N$, are non-negative. A detailed study on the conditions of a positive WVS for a harmonizable process can be found in the work by Flandrin [50].

For a quasi-stationary $\mathbf{X}(t)$ with non-negative auto-WVSes, its time-varying coherence $C_{ij}(t, f)$ between $X_i(t)$ and $X_j(t)$ is defined by [51]

$$C_{ij}(t, f) = \frac{W_{ij}(t, f)}{\sqrt{W_{ii}(t, f)W_{jj}(t, f)}}, \tag{12}$$

where $W_{ij}(t, f)$ is the ij^{th} element of $\mathbf{W}(t, f)$.

3. MTST method for WVS and Loève spectrum estimations

In this section, the orthogonal time-frequency Hermite windows [44, 45] and their related dual-time, dual-frequency, and time-frequency kernels are introduced. Subsequently, the mathematical formulas of the MTST method for the estimations of WVS and Loève spectrum are given.

3.1. Time-frequency Hermite windows

A set of orthogonal time-frequency Hermite windows $\psi_m(t, f)$ is calculated by [44, 45]

$$\psi_m(t, f) = \sqrt{w(f)}h_m\left[w(f)t\right], \tag{13}$$

where m is the order, $h_m(t)$ is the m^{th}-order Hermite function [27], and $w(f)$ is a shape function controlling the shape of $\psi_m(t, f)$. $w(f)$ is expressed as [44, 45]

$$w(f)=a\left[1+\frac{b^2\left|f/f_\mathrm{s}\right|^{|c|+1}}{|b|\left|f/f_\mathrm{s}\right|^{|c|+1}+1}\right],\tag{14}$$

where a, b, and c are three shape parameters. $w(f)$ controls the width of $\psi_m(t, f)$ at each frequency point. A larger $w(f)$ corresponds to a narrower width of $\psi_m(t, f)$. $w(f)$ is a monotonically increasing function in the frequency domain. Thus, the width of $\psi_m(t, f)$ narrows as the frequency increases. The form of $\psi_m(t, f)$ equips the MTST method with a time-frequency analysis capability similar to that of wavelet transform. The parameter a controls the width of $\psi_m(t, f)$ at f = 0 Hz. Parameters b and c jointly control the shape of $w(f)$. When b = 0, $w(f) = a$ reduces to a constant value. Consequently, $\psi_m(t, f)$ becomes a frequency-independent window. A more detailed explanation of $w(f)$ as well as a, b, and c can be found in [44].

$\psi_0(t, f)$ and $\psi_1(t, f)$ are respectively calculated as

$$\psi_0(t, f)=\pi^{-0.25}\sqrt{w(f)}e^{-0.5w^2(f)t^2}\tag{15}$$

and

$$\psi_1(t, f)=\sqrt{2}\pi^{-0.25}w^{1.5}(f)te^{-0.5w^2(f)t^2}.\tag{16}$$

The iterative calculation of high-order $\psi_m(t, f)$, $m > 1$, is

$$\psi_m(t, f)=\sqrt{\frac{2}{m}}w(f)t\psi_{m-1}(t, f)-\sqrt{\frac{m-1}{m}}\psi_{m-2}(t, f).\tag{17}$$

$\psi_m(t, f)$ with a small Δt satisfies the orthogonal condition

$$\Delta t\sum_{k=-\infty}^{+\infty}\psi_m^*(k\Delta t, f)\psi_n(k\Delta t, f)=\delta_{mn},\tag{18}$$

where δ_{mn} is the Kronecker delta symbol.

A dual-time kernel $\phi_M(t_1, t_2, f)$ formed by $\psi_m(t, f)$, $m = 0, 1,\ldots, M-1$, is calculated as

$$\phi_M(t_1,t_2, f)=\frac{1}{M}\sum_{m=0}^{M-1}\psi_m^*(t_1, f)\psi_m(t_2, f).\tag{19}$$

Since $\psi_m(t, f)$ is an even real function with respect to t for an even m and an odd real function for an odd m, $\phi_M(t_1, t_2, f)$ satisfies following symmetric conditions

$$\phi_M(t_1,t_2, f)=\phi_M(t_2,t_1, f)=\phi_M(-t_1,-t_2, f).\tag{20}$$

A dual-frequency kernel $\varphi_M(f_1, f_2, f)$, the 2D Fourier transform of $\phi_M(t_1, t_2, f)$, is calculated as

$$\varphi_M(f_1, f_2, f) = \Delta t^2 \sum_{k=-\infty}^{+\infty} \sum_{l=-\infty}^{+\infty} e^{\mathrm{i}2\pi(f_1 k - f_2 l)\Delta t} \phi_M(k\Delta t, l\Delta t, f). \tag{21}$$

Assuming

$$\varphi_M(f_1, f_2, f) = \begin{cases} \varphi_M(f_1, f_2, f), & -f_{\mathrm{N}} \le f_1, f_2 \le f_{\mathrm{N}} \\ 0, & \text{otherwise} \end{cases}, \tag{22}$$

$\phi_M(t_1, t_2, f)$ can be expressed as

$$\phi_M(k\Delta t, l\Delta t, f) = \int_{-\infty}^{+\infty} \int_{-\infty}^{+\infty} e^{\mathrm{i}2\pi(f_2 l - f_1 k)\Delta t} \varphi_M(f_1, f_2, f) \mathrm{d}f_1 \mathrm{d}f_2. \tag{23}$$

Because of the symmetric conditions in Eq. (20), $\varphi_M(f_1, f_2, f)$ is real-valued and has similar symmetric conditions

$$\varphi_M(f_1, f_2, f) = \varphi_M(f_2, f_1, f) = \varphi_M(-f_1, -f_2, f). \tag{24}$$

Rotating the frequency coordinate in $\varphi_M(f_1, f_2, f)$ by 45°, that is $\tilde{\varphi}_M(\lambda, \xi, f) = \varphi_M(\lambda - 0.5\xi, \lambda + 0.5\xi, f)$. A time-frequency kernel $\chi_M(t, \lambda, f)$, the inverse Fourier transform of $\tilde{\varphi}_M(\lambda, \xi, f)$ with respect to ξ, is calculated as

$$\chi_M(t, \lambda, f) = \int_{-\infty}^{+\infty} e^{\mathrm{i}2\pi\xi t} \tilde{\varphi}_M(\lambda, \xi, f) \mathrm{d}\xi. \tag{25}$$

$\chi_M(t, \lambda, f)$ and $\tilde{\varphi}_M(\lambda, \xi, f)$ constitute a continuous 1D Fourier transform pair with respect to t and ξ. Because of the symmetric conditions in Eq. (24), $\chi_M(t, \lambda, f)$ is real-valued and has symmetric conditions

$$\chi_M(t, \lambda, f) = \chi_M(t, -\lambda, f) = \chi_M(-t, \lambda, f). \tag{26}$$

Besides, with a small Δt, $\chi_M(t, \lambda, f)$ satisfies the normalization condition

$$\begin{aligned} &\int_{-\infty}^{+\infty} \int_{-\infty}^{+\infty} \chi_M(t, \lambda, f) \mathrm{d}t \mathrm{d}\lambda \\ &= \int_{-\infty}^{+\infty} \tilde{\varphi}_M(\lambda, 0, f) \mathrm{d}\lambda \\ &= \int_{-\infty}^{+\infty} \varphi_M(\lambda, \lambda, f) \mathrm{d}\lambda \\ &= \frac{1}{M} \sum_{m=0}^{M-1} \left[\Delta t \sum_{k=-\infty}^{+\infty} \psi_m^*(k\Delta t, f) \psi_m(k\Delta t, f) \right] \stackrel{(a)}{=} 1, \end{aligned} \tag{27}$$

where (a) is valid from Eq. (18).

3.2. WVS and Loève spectrum estimations

Given a harmonizable process $\mathbf{X}(t)$ defined by Eq. (1), its S-transform with M time-frequency Hermite windows $\psi_m(t, f)$, $m = 0, 1, \ldots, M-1$, is calculated as [52]

$$\mathbf{s}_m(t, f) = \Delta t \sum_{k=-\infty}^{+\infty} e^{-\mathrm{i}2\pi fk\Delta t} \psi_m(k\Delta t - t, f) \mathbf{X}(k\Delta t). \tag{28}$$

An estimator $\widehat{\mathbf{W}}(t, f)$ of the WVS $\mathbf{W}(t, f)$ in Eq. (9) is calculated as

$$\hat{\mathbf{W}}(t, f) = \frac{1}{M} \sum_{m=0}^{M-1} \mathbf{s}_m^*(t, f) \mathbf{s}_m^{\mathrm{T}}(t, f). \tag{29}$$

An estimator $\hat{\mathbf{S}}(f_1, f_2)$ of the Loève spectrum $\mathbf{S}(f_1, f_2)$ in Eq. (3) is calculated as

$$\hat{\mathbf{S}}(f_1, f_2) = \Delta t \sum_{k=-\lceil L[0.5(f_1+f_2)]/2 \rceil + 1}^{\lfloor L[0.5(f_1+f_2)]/2 \rfloor} e^{-\mathrm{i}2\pi(f_2 - f_1)k\Delta t} \hat{\mathbf{W}}\left[k\Delta t, 0.5(f_1 + f_2)\right], \tag{30}$$

where $\lfloor\ \rfloor$ is the floor function, $\lceil\ \rceil$ is the ceiling function, and positive $L(f)$ is the number of considered time instants at each frequency f. In real application, only a finite-length record, e.g., $\mathbf{x}(k\Delta t)$, $k = -0.5L + 1, -0.5L + 2, \ldots, 0, \ldots, 0.5L$, is available. L is the length of $\mathbf{x}(k\Delta t)$ and assumed to be even. In this situation, the WVS estimate calculated by Eq. (29) near the ends of $\mathbf{x}(k\Delta t)$ would be influenced by the edge effect. For each frequency f, an approximate valid range $[-t_{\mathrm{v}}(f),\ t_{\mathrm{v}}(f)]$, $t_{\mathrm{v}}(f) = [0.5L - L_{\mathrm{v}}(f)]\Delta t$, of $\widehat{\mathbf{W}}(t, f)$ is calculated as

$$\min L_{\mathrm{v}}(f), \ \text{s.t.} \begin{cases} L_{\mathrm{v}}(f) < 0.5L \\ \Delta t \displaystyle\sum_{k=-L_{\mathrm{v}}(f)}^{L_{\mathrm{v}}(f)} \psi_{M-1}^2(k\Delta t, f) \geq 0.9995. \\ L_{\mathrm{v}}(f) \in \mathbb{Z}^+ \end{cases} \tag{31}$$

$L(f)$ in Eq. (30) should be in the valid range, that is $L(f) + 2L_{\mathrm{v}}(f) \leq L$.

An estimator $\widehat{C}_{ij}(t, f)$ of the time-varying coherence $C_{ij}(t, f)$ in Eq. (12) is calculated as

$$\hat{C}_{ij}(t, f) = \frac{\hat{W}_{ij}(t, f)}{\sqrt{\hat{W}_{ii}(t, f)\hat{W}_{jj}(t, f)}}, \tag{32}$$

where $\widehat{W}_{ij}(t, f)$ is the ij^{th} element of $\widehat{\mathbf{W}}(t, f)$. If $C_{ij}(t, f)$ is time-invariant, which is denoted as

$$C_{ij}(t, f) = \bar{C}_{ij}(f), \tag{33}$$

an estimator $\hat{\bar{C}}_{ij}(f)$ of $\bar{C}_{ij}(f)$ is calculated as

$$\hat{\bar{C}}_{ij}(f) = \frac{1}{L(f)} \sum_{k=-\lceil L(f)/2 \rceil+1}^{\lfloor L(f)/2 \rfloor} \hat{C}_{ij}(k\Delta t, f). \tag{34}$$

By the Cauchy-Schwarz inequality, it is satisfied that $|\widehat{C}_{ij}(t, f)| \leq 1$ and $|\hat{\bar{C}}_{ij}(f)| \leq 1$, where $|\bullet|$ is the modulus operator.

The estimator $\widehat{\mathbf{W}}(t, f)$ in Eq. (29) belongs to the class of spectrograms and it is non-negative [20]. The calculation procedure of $\widehat{\mathbf{W}}(t, f)$, including Eqs. (28) and (29), is same with those of the EPSD estimator by the MTST method [45]. It has been indicated that a spectrogram can be utilized to estimate either an EPSD or a WVS [20]. However, these two target time-varying spectra are theoretically different and should be specified before an estimation.

4. Statistical properties of the WVS, Loève spectrum and coherence estimators

In this section, $\mathbf{X}(t)$ in Eq. (1) is assumed to be Gaussian. The analytical biases and variances of $\widehat{\mathbf{W}}(t, f)$ in Eq. (29), $\hat{\mathbf{S}}(f_1, f_2)$ in Eq. (30), $\widehat{C}_{ij}(t, f)$ in Eq. (32), and $\hat{\bar{C}}_{ij}(f)$ in Eq. (34) are provided.

Theorem 1: Under the Gaussianity assumption on $\mathbf{X}(t)$, at $t = k\Delta t$, the bias $\text{Bias}[\widehat{W}_{ij}(t, f)] = \text{E}[\widehat{W}_{ij}(t, f)] - W_{ij}(t, f)$ of $\widehat{W}_{ij}(t, f)$, which is the ij^{th} element of $\widehat{\mathbf{W}}(t, f)$, is calculated as

$$\text{Bias}\left[\hat{W}_{ij}(t, f)\right] = \int_{-\infty}^{+\infty}\int_{-\infty}^{+\infty} \chi_M(\tau - t, f - \xi, f)\left[W_{ij}(\tau, \xi) - W_{ij}(t, f)\right]\mathrm{d}\tau\mathrm{d}\xi, \tag{35}$$

where $\chi_M(t, \lambda, f)$ is in Eq. (25). The variance $\text{Var}[\widehat{W}_{ij}(t, f)]$ of $\widehat{W}_{ij}(t, f)$ is approximated as

$$\begin{aligned}
&\text{Var}\left[\hat{W}_{ij}(t, f)\right] \\
&\approx \int_{-\infty}^{+\infty}\int_{-\infty}^{+\infty} \tilde{\varphi}_M^*(u - f, v, f)\tilde{\varphi}_M(u - f, v, f)W_{ii}^*(t, u - 0.5v)W_{jj}(t, u + 0.5v)\mathrm{d}u\mathrm{d}v \\
&\quad + \int_{-\infty}^{+\infty}\int_{-\infty}^{+\infty} \tilde{\varphi}_M^*(f + 0.5v, 2u, f)\tilde{\varphi}_M(f - 0.5v, 2u, f)W_{ij}^*(t, u - 0.5v)W_{ij}(t, u + 0.5v)\mathrm{d}u\mathrm{d}v.
\end{aligned} \tag{36}$$

The proof of Theorem 1 is provided in Appendix A.

Corollary 1: With the conditions in Theorem 1, and $\tilde{\varphi}_M(u, v, f)$ is more concentrated compared with $W_{ii}(t,\ u+0.5v)$, $W_{jj}(t,\ u+0.5v)$ and $W_{ij}(t,\ u+0.5v)$, then Var[$\widehat{W}_{ij}(t,\ f)$] in Eq. (36) is approximately simplified as

$$\mathrm{Var}\left[\hat{W}_{ij}(t,f)\right]\approx\frac{1}{M}W_{ii}^{*}(t,f)W_{jj}(t,f)+\left|W_{ij}(t,f)\right|^{2}\int_{-\infty}^{+\infty}\int_{-\infty}^{+\infty}\tilde{\varphi}_{M}^{*}(f+v,u,f)\tilde{\varphi}_{M}(f-v,u,f)\mathrm{d}u\mathrm{d}v. \quad (37)$$

The proof of Corollary 1 is provided in Appendix B.

Remark: Martin and Flandrin [22] proposed a WVS estimator and deduced its analytical expectation and variance. The valid range of that WVS estimator in the frequency domain is [$-0.5f_{\mathrm{N}}$, $0.5f_{\mathrm{N}}$], and it is smaller than that of $\widehat{\mathbf{W}}(t,f)$ in Eq. (29), which is [$-f_{\mathrm{N}}$, f_{N}]. The second terms on right side of Eqs. (36) and (37) were ignored in the result by Martin and Flandrin [22]. In the next section, with a numerical case, it will be illustrated that the first term of Eq. (37) would undervalue the WVS estimation variances near 0 Hz and f_{N}, and the second term of Eq. (37) proposed in this study could remedy these underestimates. The result in Eq. (37) indicate that increasing M can reduce the WVS estimation variance. However, a large M could decrease the concentration of $\chi_M(t,\lambda,f)$ and increase the bias of the WVS estimation in Eq. (35).

Theorem 2: Under the Gaussianity assumption on $\mathbf{X}(t)$, the bias Bias[$\hat{S}_{ij}(f_1,\ f_2)$] = E[$\hat{S}_{ij}(f_1,\ f_2)$] – $S_{ij}(f_1,\ f_2)$ of $\hat{S}_{ij}(f_1,\ f_2)$, which is the ij^{th} element of $\hat{\mathbf{S}}(f_1,\ f_2)$, is calculated as

$$\begin{aligned}&\mathrm{Bias}\left[\hat{S}_{ij}(f_1,f_2)\right]\\&=\int_{-\infty}^{+\infty}\int_{-\infty}^{+\infty}F_{\Pi}\left[(f_2-f_1)-\lambda,0.5(f_1+f_2)\right]\tilde{\varphi}_M\left[\xi-0.5(f_1+f_2),\lambda,0.5(f_1+f_2)\right]\tilde{S}_{ij}(\xi,\lambda)\mathrm{d}\xi\mathrm{d}\lambda\\&-S_{ij}(f_1,f_2),\end{aligned} \quad (38)$$

where

$$F_{\Pi}(\lambda,f)=\begin{cases}\Delta t\sum_{k=-\infty}^{+\infty}e^{-\mathrm{i}2\pi\lambda k\Delta t}\Pi(k\Delta t,f), & |\lambda|\le f_{\mathrm{N}}\\ 0, & \text{otherwise}\end{cases} \quad (39)$$

and

$$\Pi(t,f)=\begin{cases}1, & -\lceil 0.5L(f)\rceil<t\le\lfloor 0.5L(f)\rfloor\\ 0, & \text{otherwise}\end{cases}. \quad (40)$$

The variance Var[$\hat{S}_{ij}(f_1,\ f_2)$] of $\hat{S}_{ij}(f_1,\ f_2)$ is approximated as

$$\mathrm{Var}\left[\hat{S}_{ij}(f_1, f_2)\right] \approx V_1(f_1, f_2) + V_2(f_1, f_2), \tag{41}$$

where

$$\begin{aligned} &V_1(f_1, f_2) \\ &\quad = \int_{-\infty}^{+\infty}\int_{-\infty}^{+\infty}\int_{-\infty}^{+\infty}\int_{-\infty}^{+\infty} \left|\varphi_M\left[\xi, \lambda, 0.5(f_1+f_2)\right]\right|^2 \\ &\qquad \times F_\Pi^*\left\{(f_2 - f_1) - \left[\lambda - \xi + 0.5(\Delta\xi - \Delta\lambda)\right], 0.5(f_1+f_2)\right\} \\ &\qquad \times F_\Pi\left\{(f_2 - f_1) - \left[\lambda - \xi + 0.5(\Delta\lambda - \Delta\xi)\right], 0.5(f_1+f_2)\right\} \\ &\qquad \times \tilde{S}_{ii}^*\left[0.5(f_1+f_2), \Delta\xi\right]\tilde{S}_{jj}\left[0.5(f_1+f_2), \Delta\lambda\right] \mathrm{d}\Delta\xi \mathrm{d}\Delta\lambda \mathrm{d}\xi \mathrm{d}\lambda, \end{aligned} \tag{42}$$

$$\begin{aligned} &V_2(f_1, f_2) \\ &\quad = \int_{-\infty}^{+\infty}\int_{-\infty}^{+\infty} \varphi_M^*\left[\xi - 0.5(f_1+f_2), \lambda - 0.5(f_1+f_2), 0.5(f_1+f_2)\right] \\ &\qquad \times \varphi_M\left[\xi + 0.5(f_1+f_2), \lambda + 0.5(f_1+f_2), 0.5(f_1+f_2)\right] v_{ij}(\lambda, \xi, f_1, f_2) \mathrm{d}\xi \mathrm{d}\lambda, \end{aligned} \tag{43}$$

and

$$\begin{aligned} &v_{ij}(\lambda, \xi, f_1, f_2) \\ &\quad = \int_{-\infty}^{+\infty}\int_{-\infty}^{+\infty} F_\Pi^*\left[(f_2 - f_1) - (\lambda - \xi) + 0.5(\Delta\lambda - \Delta\xi), 0.5(f_1+f_2)\right] \\ &\qquad \times F_\Pi\left[(f_2 - f_1) - (\lambda - \xi) - 0.5(\Delta\lambda - \Delta\xi), 0.5(f_1+f_2)\right]\tilde{S}_{ij}^*(\xi, \Delta\xi)\tilde{S}_{ji}(\lambda, \Delta\lambda) \mathrm{d}\Delta\xi \mathrm{d}\Delta\lambda. \end{aligned} \tag{44}$$

The proof of Theorem 2 is provided in Appendix C.

Theorem 3: Under the conditions that $\mathbf{X}(t)$ is Gaussian, the time of stationarity of $\mathbf{X}(t)$ is larger than the width of the utilized windows $\psi_m(t, f)$, $m = 0, 1, \ldots, M - 1$, and $\widehat{\mathbf{W}}(t, f)$ is approximately unbiased, the bias $\mathrm{Bias}[\widehat{C}_{ij}(t, f)] = \mathrm{E}[\widehat{C}_{ij}(t, f)] - C_{ij}(t, f)$ of $\widehat{C}_{ij}(t, f)$ is approximated as

$$\mathrm{Bias}\left[\hat{C}_{ij}(t, f)\right] \approx C_{ij}(t, f)\left[G_{ij}(t, f) - 1\right], \tag{45}$$

where $C_{ij}(t, f)$ is the theoretical coherence in Eq. (12),

$$G_{ij}(t, f) \approx \frac{\Gamma^2(M + 0.5)}{\Gamma^2(M)M}\left[1 - \left|C_{ij}(t, f)\right|^2\right]^M {}_2F_1\left[M + 0.5, M + 0.5, M + 1; \left|C_{ij}(t, f)\right|^2\right], \tag{46}$$

$\Gamma(\bullet)$ is the Gamma function and ${}_2F_1$ is the two-one hypergeometric function

$${}_2F_1(a, b; c; z) = \sum_{k=0}^{\infty} \frac{\Gamma(a+k)\Gamma(b+k)\Gamma(c)z^k}{\Gamma(a)\Gamma(b)\Gamma(c+k)k!}. \tag{47}$$

$\mathrm{Bias}[|\widehat{C}_{ij}(t, f)|] = \mathrm{E}[|\widehat{C}_{ij}(t, f)|] - |C_{ij}(t, f)|$ of $|\widehat{C}_{ij}(t, f)|$ is approximated as

$$\begin{aligned}&\mathrm{Bias}\left[\left|\hat{C}_{ij}(t,f)\right|\right]\\&\approx\frac{\Gamma(M)\sqrt{\pi}}{2\Gamma(M+0.5)}\left[1-\left|C_{ij}(t,f)\right|^2\right]^M {}_3F_2\left[1.5,M,M;1,M+0.5;\left|C_{ij}(f)\right|^2\right]-\left|C_{ij}(t,f)\right|,\end{aligned}\tag{48}$$

where ${}_3F_2$ is the three-two hypergeometric function

$${}_3F_2(a,b,c;d,e;z)=\sum_{k=0}^{\infty}\frac{\Gamma(a+k)\Gamma(b+k)\Gamma(c+k)\Gamma(d)\Gamma(e)z^k}{\Gamma(a)\Gamma(b)\Gamma(c)\Gamma(d+k)\Gamma(e+k)k!}.\tag{49}$$

$\mathrm{Var}[\hat{C}_{ij}(t,f)]$ of $\hat{C}_{ij}(t,f)$ is approximated as

$$\mathrm{Var}\left[\hat{C}_{ij}(t,f)\right]\approx\frac{1}{M}\left[1-\left|C_{ij}(t,f)\right|^2\right]^M {}_3F_2\left[2,M,M;M+1,1;\left|C_{ij}(t,f)\right|^2\right]-\left|C_{ij}(t,f)\right|^2 G_{ij}^2(t,f).\tag{50}$$

The proof of Theorem 3 is provided in Appendix D.

Theorem 4: Under the conditions that $\mathbf{X}(t)$ is Gaussian, the time of stationarity of $\mathbf{X}(t)$ is larger than the width of the utilized windows $\psi_m(t,f)$, $m = 0, 1, \ldots, M-1$, the coherence between $X_i(t)$ and $X_j(t)$ is time-invariant, and $\widehat{\mathbf{W}}(t,f)$ is approximately unbiased, the bias $\mathrm{Bias}[\hat{\bar{C}}_{ij}(f)] = \mathrm{E}[\hat{\bar{C}}_{ij}(f)] - \bar{C}_{ij}(f)$ of $\hat{\bar{C}}_{ij}(f)$ is approximated as

$$\mathrm{Bias}\left[\hat{\bar{C}}_{ij}(f)\right]\approx\bar{C}_{ij}(f)\left[T_{ij}(f)-1\right],\tag{51}$$

where

$$T_{ij}(f)\approx\frac{\Gamma^2(M+0.5)}{\Gamma^2(M)M}\left[1-\left|\bar{C}_{ij}(f)\right|^2\right]^M {}_2F_1\left[M+0.5,M+0.5,M+1;\left|\bar{C}_{ij}(f)\right|^2\right].\tag{52}$$

The variance $\mathrm{Var}[\hat{\bar{C}}_{ij}(f)]$ of $\hat{\bar{C}}_{ij}(f)$ is approximated as

$$\mathrm{Var}\left[\hat{\bar{C}}_{ij}(f)\right]\approx\frac{1}{N_{\mathrm{eq}}(f)}\left\{\frac{1}{M}\left[1-\left|\bar{C}_{ij}(f)\right|^2\right]^M {}_3F_2\left[2,M,M;M+1,1;\left|\bar{C}_{ij}(f)\right|^2\right]-\left|\bar{C}_{ij}(f)\right|^2 T_{ij}^2(f)\right\},\tag{53}$$

where

$$N_{\mathrm{eq}}(f)=\frac{L(f)}{L_{\mathrm{v}}(f)}\tag{54}$$

and $L_{\mathrm{v}}(f)$ is in Eq. (31). The proof of Theorem 4 is provided in Appendix E.

5. Verification of the MTST method for the WVS and Loève spectrum estimations

In this section, the reliability of the MTST method is verified using a bivariate harmonizable wind speed process $\mathbf{U}(t) = [U_1(t),\ U_2(t)]^{\mathrm{T}}$. The WVS matrix $\mathbf{W}_{\mathbf{U}}(t, f)$ of $\mathbf{U}(t)$ is expressed as

$$\mathbf{W}_{\mathbf{U}}(t, f) = \begin{bmatrix} W_{U_1}(t, f) & r_{\mathbf{U}}(t, f)\sqrt{W_{U_1}(t, f)W_{U_2}(t, f)} \\ r_{\mathbf{U}}^{*}(t, f)\sqrt{W_{U_1}(t, f)W_{U_2}(t, f)} & W_{U_2}(t, f) \end{bmatrix}. \quad (55)$$

In Eq. (55), $W_{U_1}(t, f) = W_U(t - 1700, f)$, $W_{U_2}(t, f) = W_U(t - 2300, f)$, $W_U(t, f)$ is [45]

$$W_U(t, f) = A^2(t, f)\frac{320}{\left(1 + 1770 f^2\right)^{5/6}}, \quad (56)$$

and

$$A(t, f) = 0.2e^{-0.000001t^2} + 1.54\left|f\right|^{0.945} e^{-\left|f\right|^{0.63} 0.000144t^2}. \quad (57)$$

The time-varying coherence $r_{\mathbf{U}}(t, f)$ is expressed as

$$r_{\mathbf{U}}(t, f) = \left[1 - 5\upsilon(f)\right]e^{\mathrm{i}fd(t) - 10\upsilon(f)}, \quad (58)$$

where

$$d(t) = 10\sin(0.001\pi t) \quad (59)$$

and

$$\upsilon(f) = \sqrt{0.1f^2 + 10^{-4}}. \quad (60)$$

The theoretical Loève spectra $S_{U_1}(f_1,\ f_2)$ and $S_{U_2}(f_1,\ f_2)$ of $U_1(t)$ and $U_2(t)$ can be calculated by 1D Fourier transform of $W_{U_1}(t, f)$ and $W_{U_2}(t, f)$ with respect to t, respectively. The theoretical correlation of $\mathbf{U}(t)$ can be calculated by the inverse Fourier transform of $\mathbf{W}_{\mathbf{U}}(t, f)$ with respect to f. The realizations of $\mathbf{U}(t)$ can be simulated by decomposing its correlation matrix [15]. In this section, all the methods employed for spectrum estimations have their own parameters requiring manual determination. For all the spectrum estimations in this section, the parameters of all methods are manually determined so that the respective method can provide its best result.

5.1. WVS and Loève spectrum estimations based on one set of realizations.

A set of simulated discrete-time realizations $[u_1(t),\ u_2(t)]^{\mathrm{T}}$, $t = 0, 1, \ldots, 3999$ s, are shown in Fig.

1. Based on these two realizations, $W_{U_1}(t, f)$ and $W_{U_2}(t, f)$ are estimated by the MTST method, multi-taper WVS estimation method [27], and Toeplitz kernel method [29]. The multi-taper method is a simplified version of the MTST with a set of original Hermite windows. The Toeplitz kernel method first calculates the spectrogram of a realization using a single time window, and then applies a smoothing window to smooth this spectrogram along the frequency axis. In the MTST method, the first ten time-frequency Hermite windows with a = 0.0125, b = 9.2, and c = 0.272 are used. In the multi-taper method, the first ten original Hermite windows, which are obtained by setting $w(f)$ in Eq. (13) as $w(f)$ = 0.05, are utilized. In the Toeplitz kernel method, the first Hermite window utilized in the multi-taper method is employed to calculate the spectrogram, and then a Gaussian window $w_g(f) = 50/\sqrt{2\pi}\mathrm{e}^{-1250f^2}$ is employed to smooth the spectrogram.

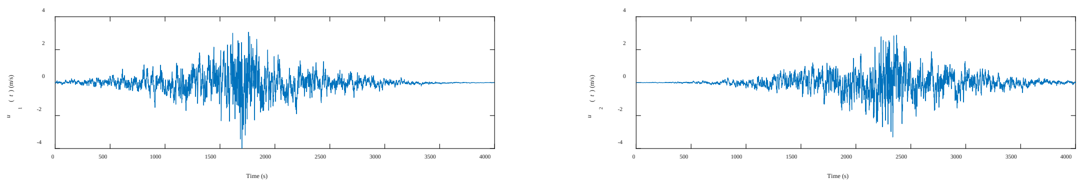

(a) (b)

Fig. 1. A set of realizations of the bivariate harmonizable wind speed process. (a) $u_1(t)$ and (b) $u_2(t)$.

Fig. 2 displays the WVS estimates by the three methods in the range of 1000 s to 3000 s, in which the estimates are not influenced by the edge effect. It is illustrated that the two WVS estimates from the MTST method have similar shapes with their corresponding theoretical ones, and their fluctuations are moderate. The results by the multi-taper method and Toeplitz kernel method have larger fluctuations compared with those by the MTST method. The mean squared error (MSE) of one WVS estimate $\widehat{W}(t, f)$ over the frequency is calculated as

$$\mathrm{MSE}(f) = \int \left[\hat{W}(t, f) - W_U(t, f)\right]^2 \mathrm{d}t, \tag{61}$$

where $W_U(t, f)$ is the corresponding theoretical one of $\widehat{W}(t, f)$. The MSEs of the WVS estimates in Fig. 2 by the three methods are displayed in Fig. 3. It is illustrated that the results by the multi-taper method have larger MSEs than those by the MTST method in the frequency range of 0.0005 Hz to 0.01 Hz. The MSEs of the results from the Toeplitz kernel method are much larger than those from the other two methods. The smoothing effect of the spectrally-smoothed spectrogram in the Toeplitz kernel method is worse than that of the estimator from the multi-taper method. Thus, the WVS estimates by the Toeplitz kernel method have larger fluctuations compared with the results by the multi-taper method. These larger fluctuations cause the larger MSEs illustrated in Fig. 3. Utilizing frequency-invariant windows, the multi-taper method suffers from limited time-frequency resolution and thus the MSEs of its results are larger than those of the MTST method.

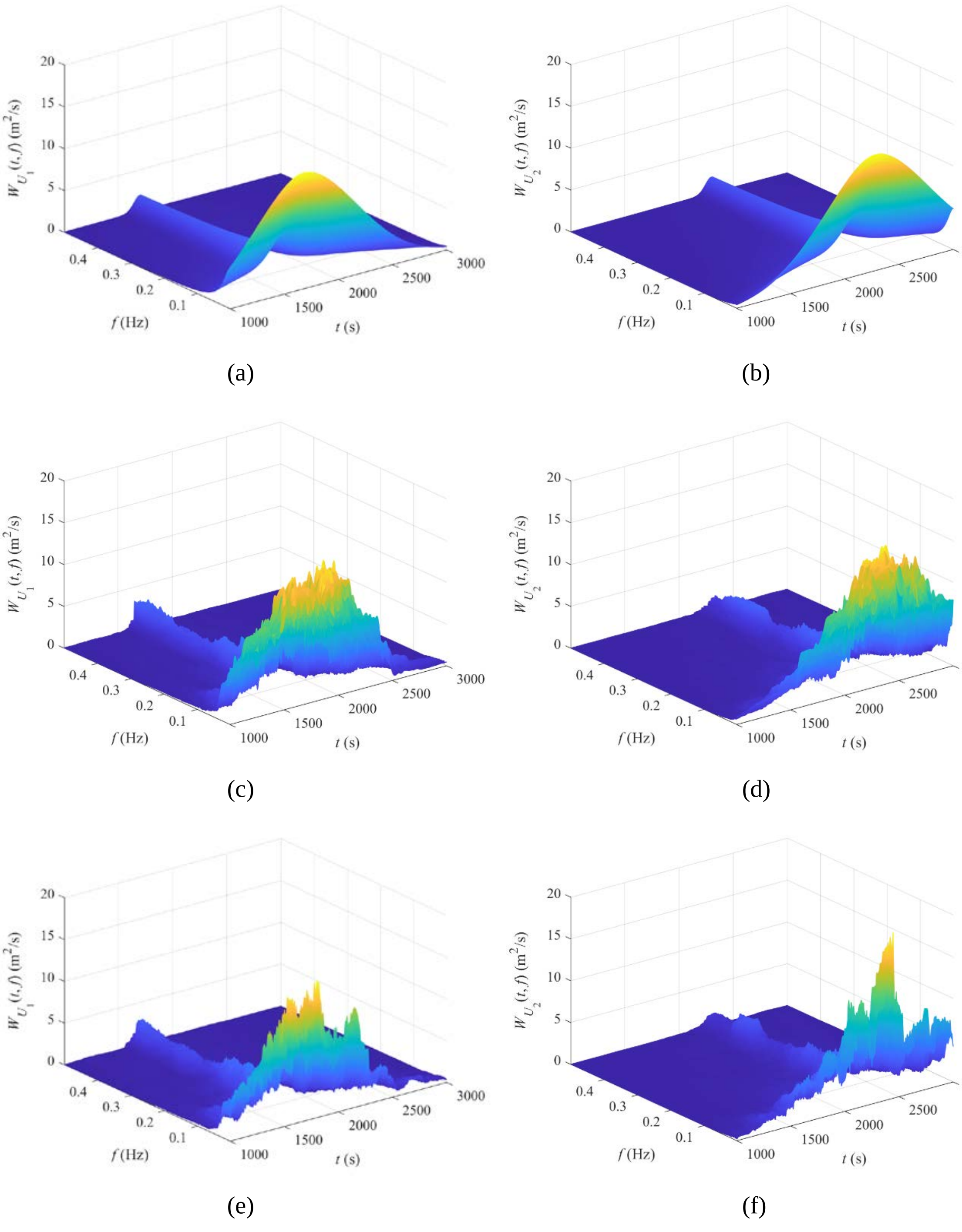

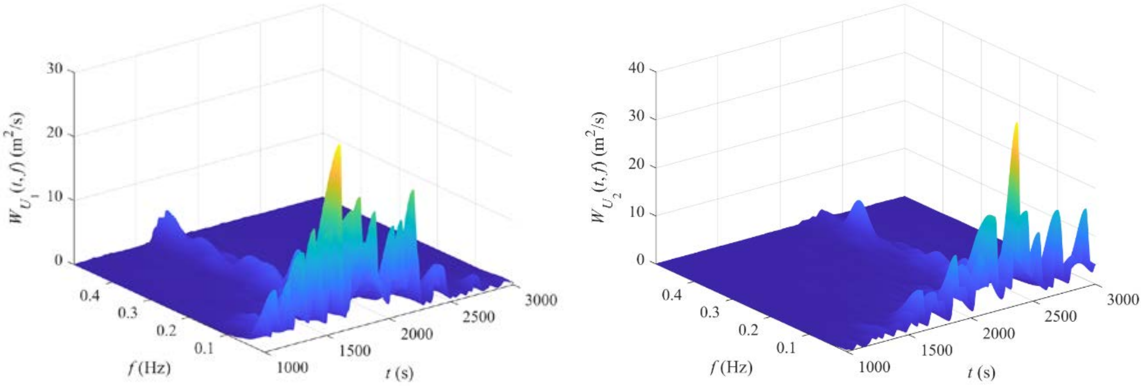

(g) (h)

Fig. 2. $W_{U_1}(t, f)$ and $W_{U_2}(t, f)$. (a) theoretical $W_{U_1}(t, f)$, (b) theoretical $W_{U_2}(t, f)$, (c) $W_{U_1}(t, f)$ by the MTST method, (d) $W_{U_2}(t, f)$ by the MTST method, (e) $W_{U_1}(t, f)$ by the multi-taper method, (f) $W_{U_2}(t, f)$ by the multi-taper method, (g) $W_{U_1}(t, f)$ by the Toeplitz kernel method, and (h) $W_{U_2}(t, f)$ by the Toeplitz kernel method.

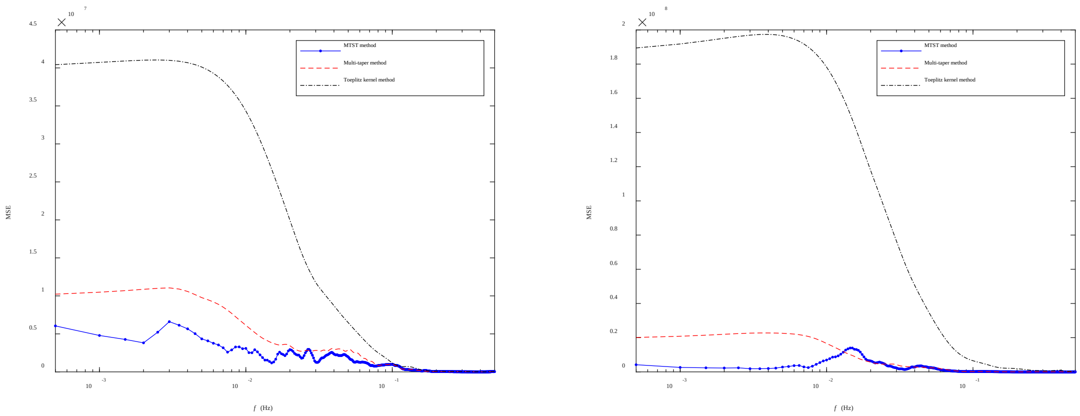

(a) (b)

Fig. 3. MSEs of the estimates of $W_{U_1}(t, f)$ and $W_{U_2}(t, f)$. (a) MSE of the estimate of $W_{U_1}(t, f)$ and (b) MSE of the estimate of $W_{U_2}(t, f)$.

The time-varying coherence $r_{\mathbf{U}}(t, f)$ is estimated by the MTST method using Eq. (32). As illustrated in Fig. 4, the real and imaginary parts of the coherence estimate could broadly exhibit the time-varying trend of $r_{\mathbf{U}}(t, f)$, but have significant fluctuations. Recently, in the EPSD estimation by the MTST method, an iterative procedure was proposed to determine the optimal number of tapers at each frequency and accordingly decrease the fluctuation in time-varying coherence estimates [46, 53]. This procedure has the potential to be applied in the time-varying coherence estimation of harmonizable processes. However, this application needs several additional works, e.g., deducing the theoretical expression of the optimal number of tapers at each frequency, and it is beyond the scope of this study.

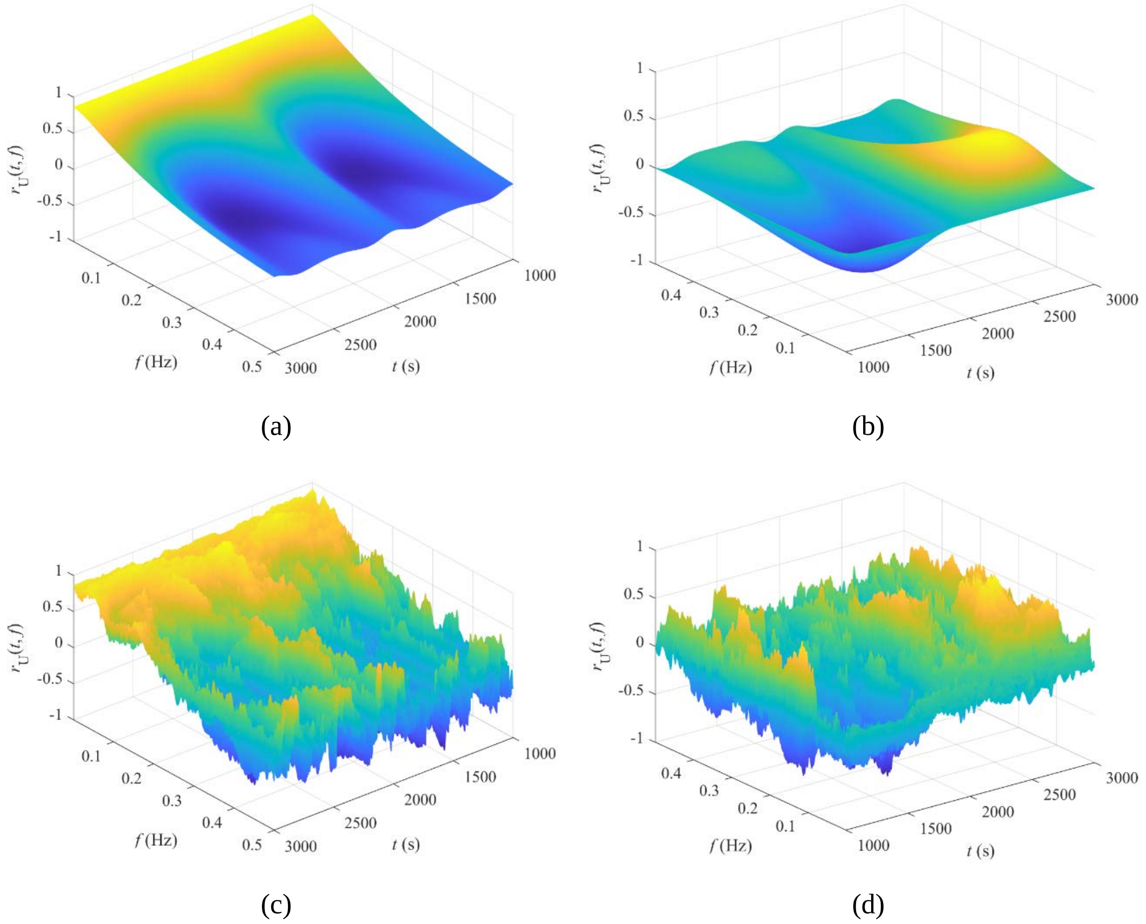

Fig. 4. $r_{\mathbf{U}}(t, f)$. (a) real part of the theoretical $r_{\mathbf{U}}(t, f)$, (b) imaginary part of the theoretical $r_{\mathbf{U}}(t, f)$, (c) real part of the estimated $r_{\mathbf{U}}(t, f)$, and (d) imaginary part of the estimated $r_{\mathbf{U}}(t, f)$.

Based on the realization $u_1(t)$, its Loève spectrum $S_{U_1}(f_1,\ f_2)$ is estimated by the MTST method, the multi-taper Loève spectrum estimation method [35, 36], and the CMS method [38, 39]. This multi-taper method used for the Loève spectrum estimation is different from the aforementioned multi-taper WVS estimation method. In the multi-taper method of Loève spectrum estimation, the first ten discrete prolate spheroidal sequences are utilized. In the CMS method, its first step is the same as that in the Toeplitz kernel method, which is to calculate the spectrogram of a realization using a single time window. Subsequently, the Loève spectrum is estimated by performing a 1D Fourier transform on the spectrogram along the time axis. The single time window in the CMS method is the same as that in the the Toeplitz kernel method.

As shown in Fig. 5, the theoretical $S_{U_1}(f_1,\ f_2)$, including its real and imaginary parts, is concentrated near the main diagonal line of $f_1 = f_2$. The result from the MTST method could clearly exhibit the pattern of $S_{U_1}(f_1,\ f_2)$ near the main diagonal line with small fluctuations. The Loève spectrum estimate from the CMS method has larger fluctuations than that from the MTST method. The result from the multi-taper method has large fluctuations over the whole dual-frequency plane and cannot display the shape of $S_{U_1}(f_1,\ f_2)$. Estimated spectrum slices of the real part of $S_{U_1}(f_1,\ f_2)$ along the lines of $f_1 = f_2$ and $f_1 = f_2 + 0.00025$ are shown in Fig. 6. Estimated spectrum slices of the imaginary part of $S_{U_1}(f_1,\ f_2)$ along the lines of $f_1 = f_2 + 0.00025$ and $f_1 = f_2 + 0.0005$ are shown Fig. 7. It is illustrated that the spectrum slices from the MTST method are close to the theoretical values with smaller fluctuations than those from the other two methods. The MSE of one Loève spectrum estimate $\hat{S}(f_1,\ f_2)$ is calculated as

$$\mathrm{MSE}_{\hat{S}} = \iint \left[\hat{S}(f_1, f_2) - S_U(f_1, f_2) \right]^2 \mathrm{d}f_1 \mathrm{d}f_2, \tag{62}$$

where $S_U(f_1,\ f_2)$ is the theoretical one of $\hat{S}(f_1,\ f_2)$. The MSEs of the Loève spectrum estimates by the MTST method, CMS method, and multi-taper method are 131. 90, 2.18×10^3, and 2.01×10^5, respectively. The MSE from the MTST method is much smaller than those from the other two methods.

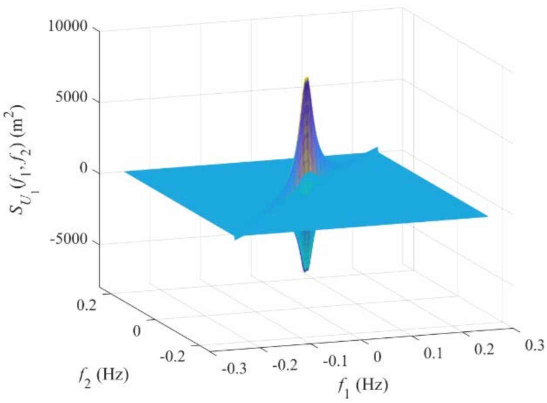

(a)

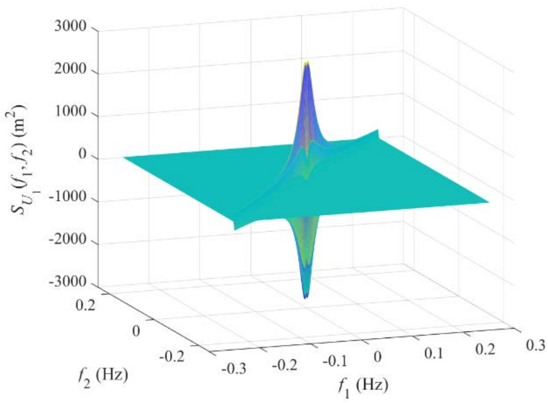

(b)

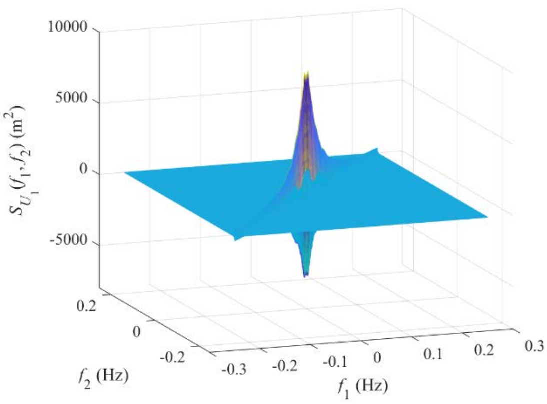

(c)

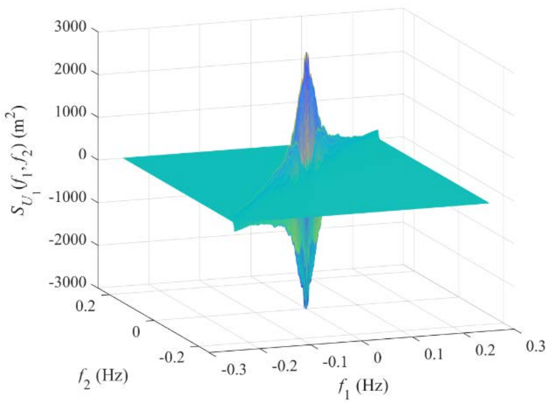

(d)

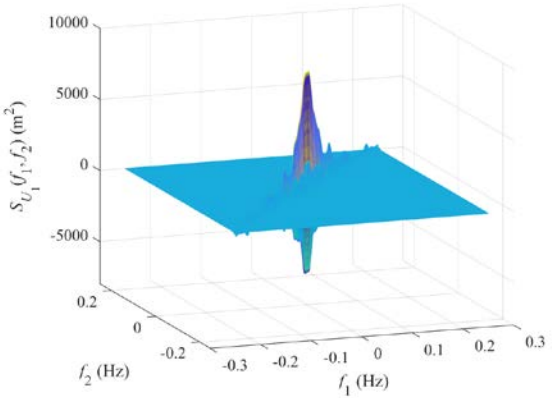

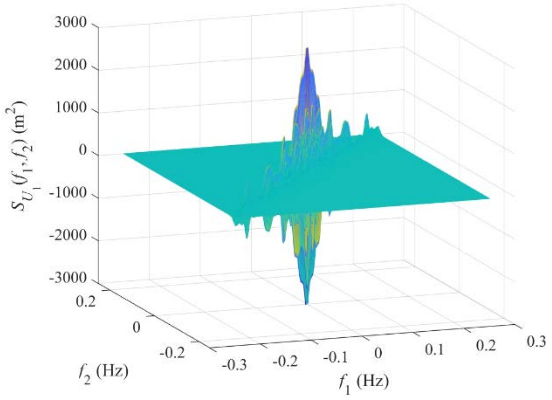

(e) (f)

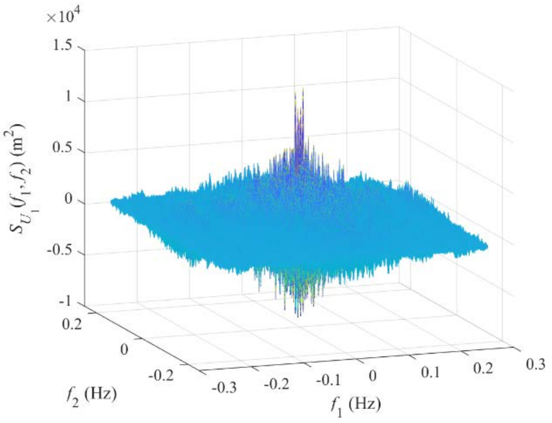

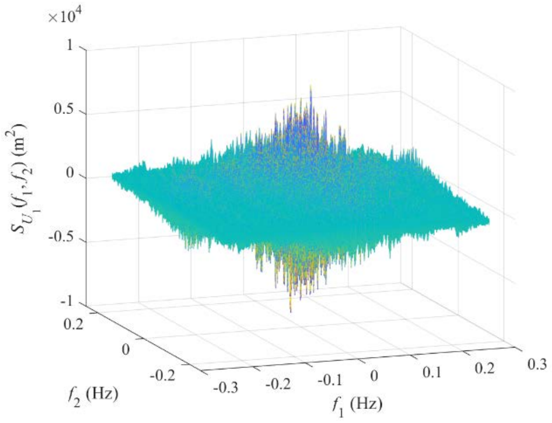

(g) (h)

Fig. 5. $S_{U_1}(f_1, f_2)$. (a) real part of the theoretical $S_{U_1}(f_1, f_2)$, (b) imaginary part of the theoretical $S_{U_1}(f_1, f_2)$, (c) real part of $S_{U_1}(f_1, f_2)$ estimated by the MTST method, (d) imaginary part of $S_{U_1}(f_1, f_2)$ estimated by the MTST method, (e) real part of $S_{U_1}(f_1, f_2)$ estimated by the CMS method, (f) imaginary part of $S_{U_1}(f_1, f_2)$ estimated by the CMS method, (g) real part of $S_{U_1}(f_1, f_2)$ estimated by the multi-taper method, and (h) imaginary part of $S_{U_1}(f_1, f_2)$ estimated by the multi-taper method.

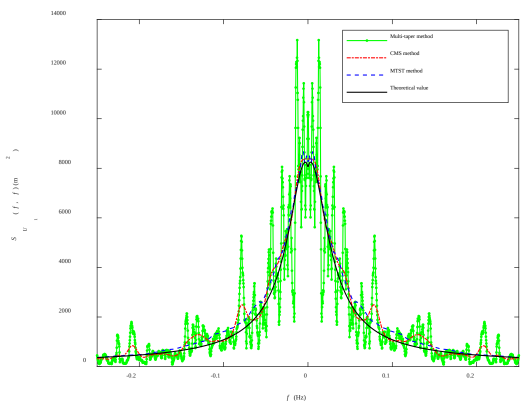

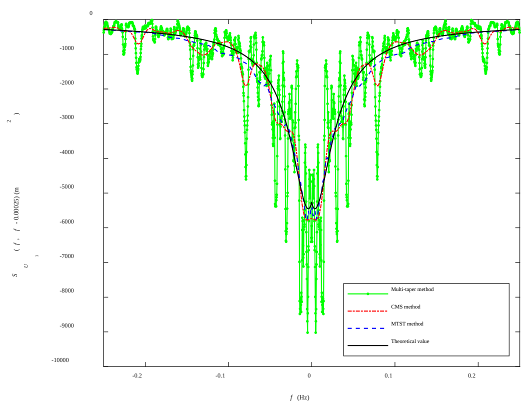

(a) (b)

Fig. 6. Estimated spectrum slices of the real part of $S_{U_1}(f_1, f_2)$. (a) the spectrum slice along the line of $f_1 = f_2$ and (b) the spectrum slice along the line of $f_1 = f_2 + 0.00025$.

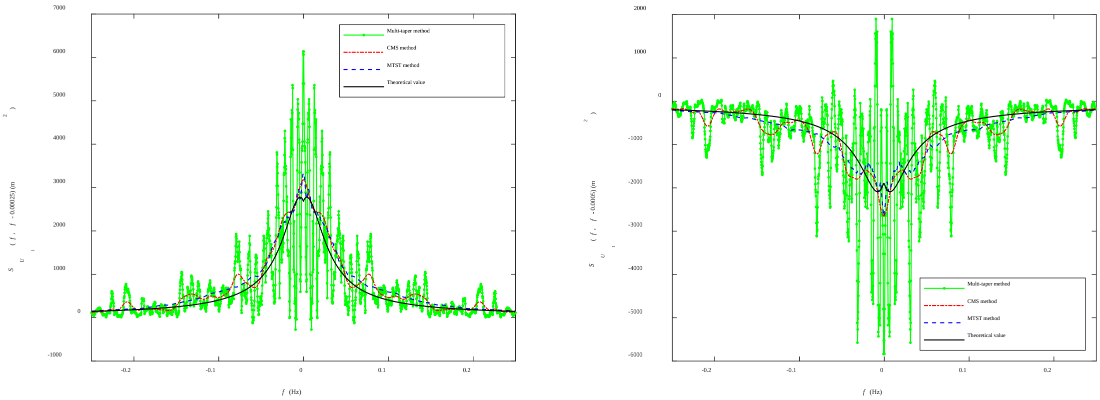

(a) (b)

Fig. 7. Estimated spectrum slices of the imaginary part of $S_{U_1}(f_1, f_2)$. (a) the spectrum slice along the line of $f_1 = f_2 + 0.00025$ and (b) the spectrum slice along the line of $f_1 = f_2 + 0.0005$.

In order to deliberate on the feasibility of the MTST method on non-Gaussian realizations, the Gaussian realizations $u_1(t)$ and $u_2(t)$ in Fig. 1 are transformed into two non-Gaussian realizations by

$$\mu_i(t) = G^{-1}\left\{\Phi\left[u_i(t), \sigma_{U_i}(t)\right], \sigma_{U_i}(t)\right\} - \sqrt{2}\sigma_{U_i}(t), \tag{63}$$

where $\Phi[\bullet, \sigma_{U_i}(t)]$ is a zero-mean Gaussian cumulative distribution function (CDF) with a standard deviation of $\sigma_{U_i}(t)$, $\sigma_{U_i}(t)$ is the time-varying standard deviation of $U_i(t)$, $G^{-1}[\bullet, \sigma_{U_i}(t)]$ is the inverse CDF of a Gamma distribution with an expectation of $\sqrt{2}\sigma_{U_i}(t)$ and a standard deviation of $\sigma_{U_i}(t)$, and i = 1 and 2. The realizations $\mu_1(t)$ and $\mu_2(t)$ are shown in Fig. 8. According to Sklar's theorem [54], the probabilistic dependence among multiple random variables is independent of their marginal PDFs. Thus, the theoretical correlation functions, WVSes, and Loève spectra of $\mu_1(t)$ and $\mu_2(t)$ are the same as those of the Gaussian realizations $u_1(t)$ and $u_2(t)$.

Two WVSes estimated by the proposed MTST method using $\mu_1(t)$ and (b) $\mu_2(t)$ are displayed in Fig. 9. It is illustrated that the two WVS estimates from the non-Gaussian realizations are also consistent with their corresponding theoretical WVSes with moderate fluctuations. The real and imaginary parts of $S_{U_1}(f_1, f_2)$ estimated by the MTST method using $\mu_1(t)$ are shown in Fig. 10. It is illustrated that the real part of the estimated $S_{U_1}(f_1, f_2)$ from the non-Gaussian realization is similar to that from the Gaussian realization in Fig. 5. The imaginary part of the Loève spectrum from the non-Gaussian realization has slightly larger fluctuations than that from the Gaussian realization in Fig. 5. The MSE of the estimated $S_{U_1}(f_1, f_2)$ from the non-Gaussian realization is 205.43, which is a little larger than the MSE of 131. 90 from the Gaussian realization.

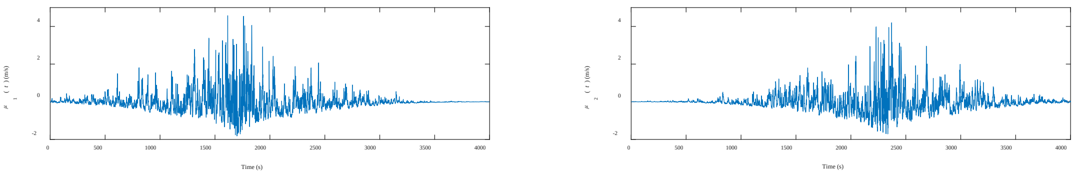

(a) (b)

Fig. 8. A set of non-Gaussian realizations of the bivariate harmonizable wind speed process. (a) $\mu_1(t)$ and (b) $\mu_2(t)$.

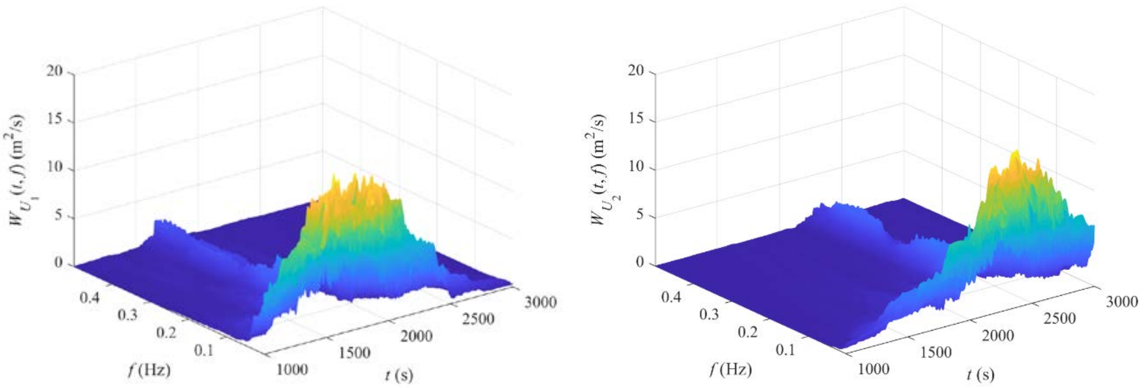

(a) (b)

Fig. 9. $W_{U_1}(t, f)$ and $W_{U_2}(t, f)$ estimated by the MTST method using $\mu_1(t)$ and $\mu_2(t)$. (a) $W_{U_1}(t, f)$ and (b) $W_{U_2}(t, f)$.

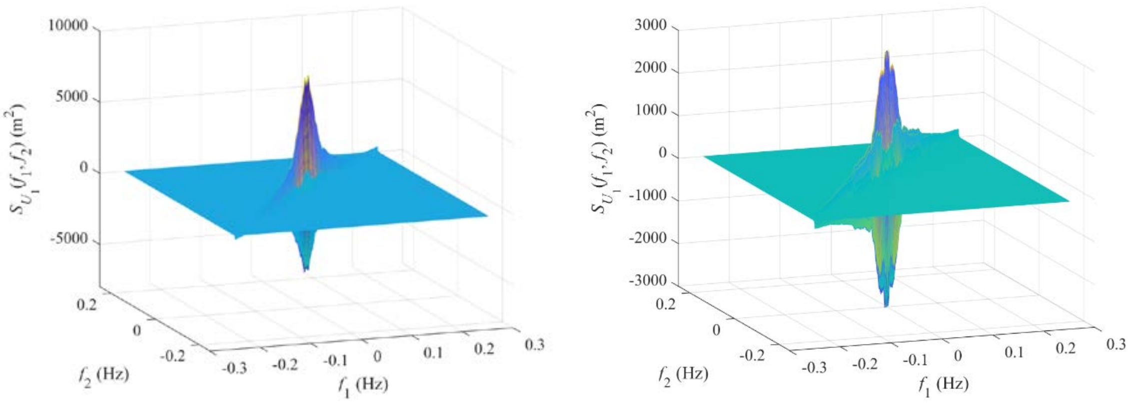

(a) (b)

Fig. 10. $S_{U_1}(f_1, f_2)$ estimated by the MTST method using $\mu_1(t)$. (a) real part of $S_{U_1}(f_1, f_2)$ and (b) imaginary part of $S_{U_1}(f_1, f_2)$,

5.2. WVS and Loève spectrum estimations based on multiple sets of realizations.

In this sub-section, 5000 sets of discrete-time realizations of $\mathbf{U}(t)$ are simulated. Averaged $W_{U_1}(t, f)$, $W_{U_2}(t, f)$, $r_{\mathbf{U}}(t, f)$, and $S_{U_1}(f_1, f_2)$ over the 5000 sets of realizations are estimated by the MTST method, in which, the first two time-frequency Hermite windows with $a = 0.015$, $b = 7$, and $c = 0.5$ are used. As illustrated in Fig. 11 to Fig. 13, the estimated WVSes coherence, and Loève spectrum are very similar to their corresponding theoretical ones. The two Loève spectrum slices in Fig. 13 only have small differences from their corresponding theoretical ones near $f = 0$ Hz.

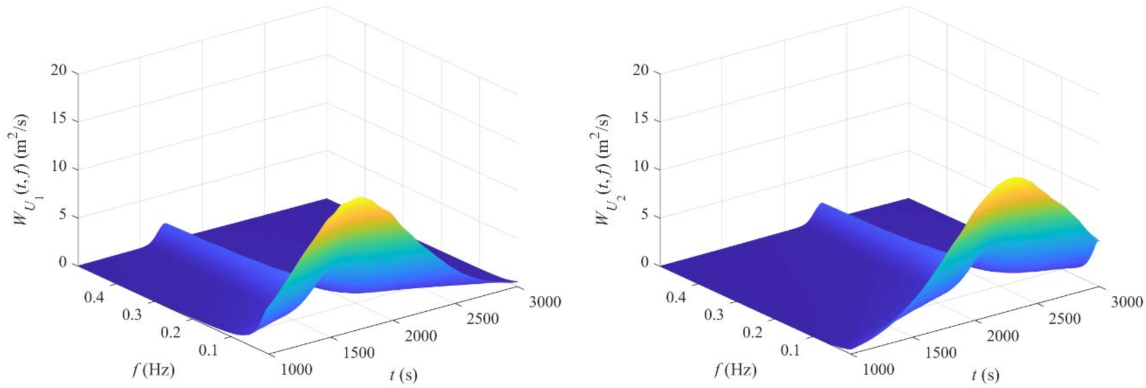

(a) (b)

Fig. 11. Averaged $W_{U_1}(t, f)$ and $W_{U_2}(t, f)$ from 5000 realizations. (a) $W_{U_1}(t, f)$ and (b) $W_{U_2}(t, f)$.

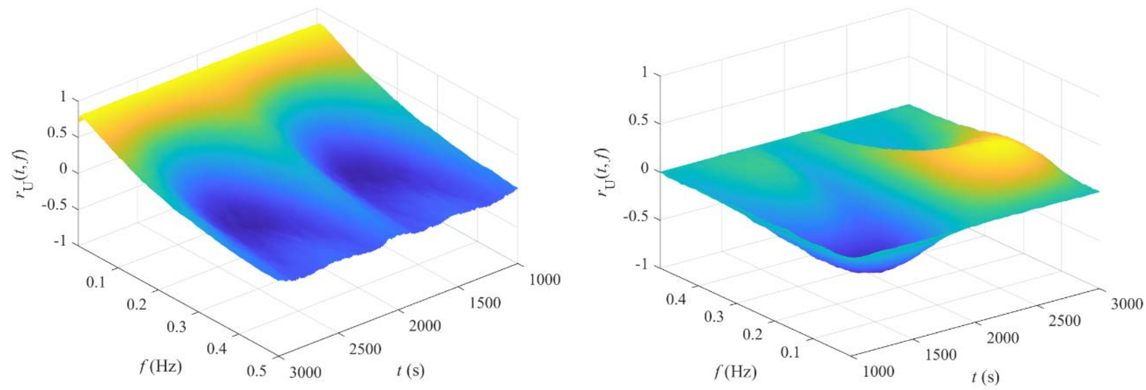

(a) (b)

Fig. 12. Averaged $r_{\mathbf{U}}(t, f)$ from 5000 realizations. (a) real part of $r_{\mathbf{U}}(t, f)$ and (b) imaginary part of $r_{\mathbf{U}}(t, f)$.

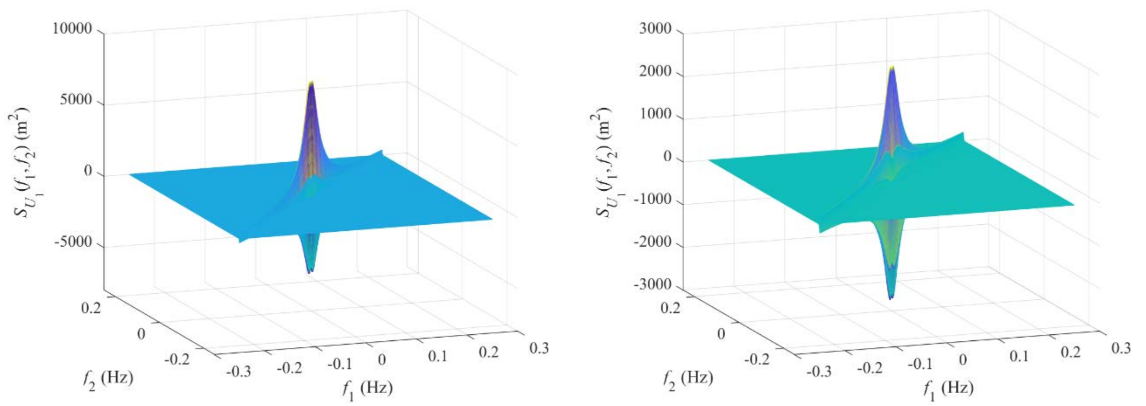

(a) (b)

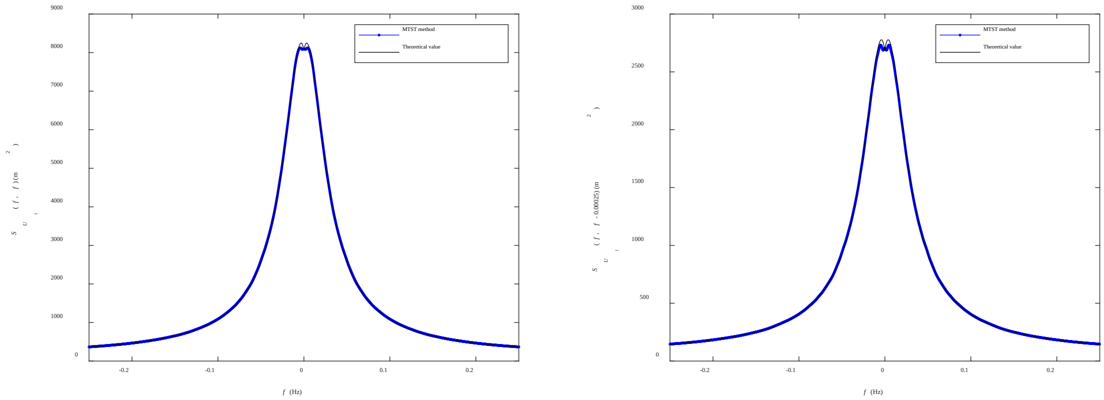

(c) (d)

Fig. 13. Averaged $S_{U_1}(f_1,\ f_2)$ from 5000 realizations. (a) real part of $S_{U_1}(f_1,\ f_2)$, (b) imaginary part of $S_{U_1}(f_1,\ f_2)$, (c) real part of the spectrum slice $S_{U_1}(f, f)$, and (d) imaginary part of the spectrum slice $S_{U_1}(f, f-0.00025)$.

The estimation variances of $W_{U_1}(t, f)$ and $r_{\mathbf{U}}(t, f)$ are calculated using the analytical expressions in Eqs. (37) and (50), respectively, and are compared with their corresponding results calculated from the 5000 realizations in Fig. 14 and Fig. 15, respectively. It can be seen the estimation variance of WVS and that of coherence from the analytical expressions are consistent with their corresponding results from the 5000 realizations. The analytical expression of the WVS estimation variance proposed by Martin and Flandrin [22] only contains the first term on the right side of Eq. (37). In Fig. 14 (c) and (d), the variances at $t = 1700$ s and $f = 0.001$ Hz by the first term of Eq. (37) are also provided. It is illustrated that the first term of Eq. (37) would undervalue the variances near 0 Hz and f_{N}, and the second term of Eq. (37) proposed in this study could remedy these underestimates.

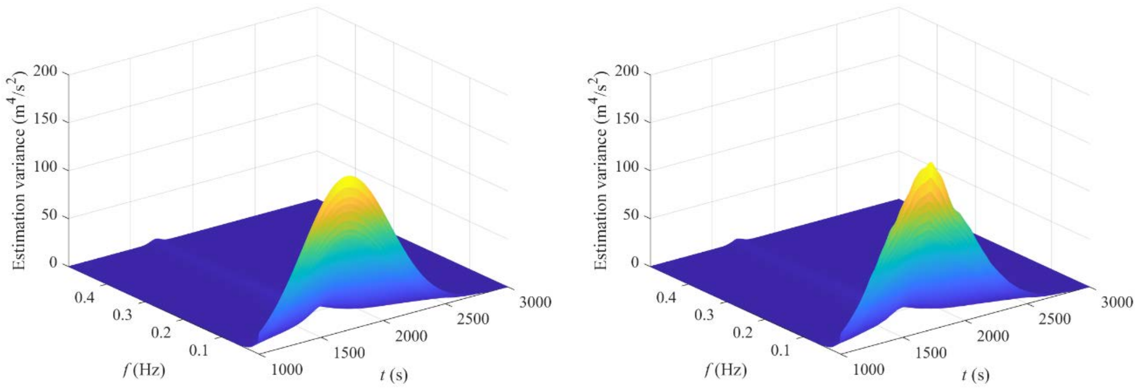

(a) (b)

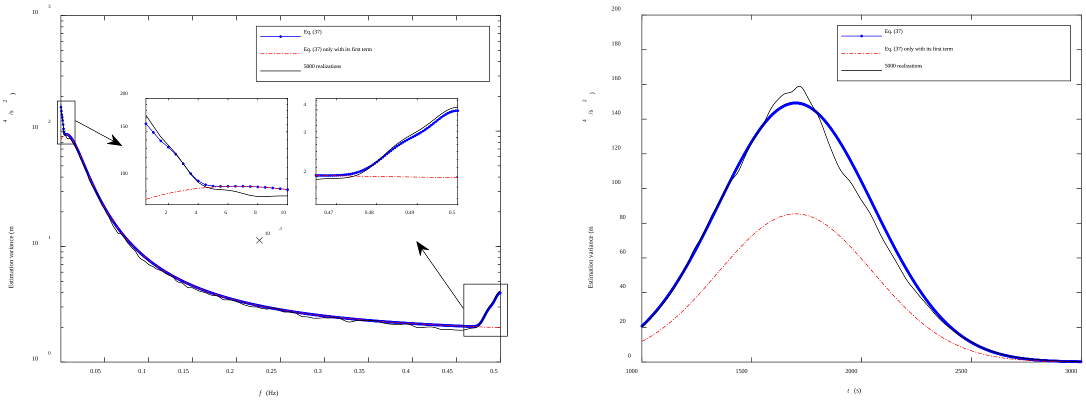

(c) (d)

Fig. 14. Estimation variance of $W_{U_1}(t, f)$. (a) the result from Eq. (37), (b) the result from the 5000 realizations, (c) the results at t = 1700 s, and (d) the results at f = 0.001 Hz.

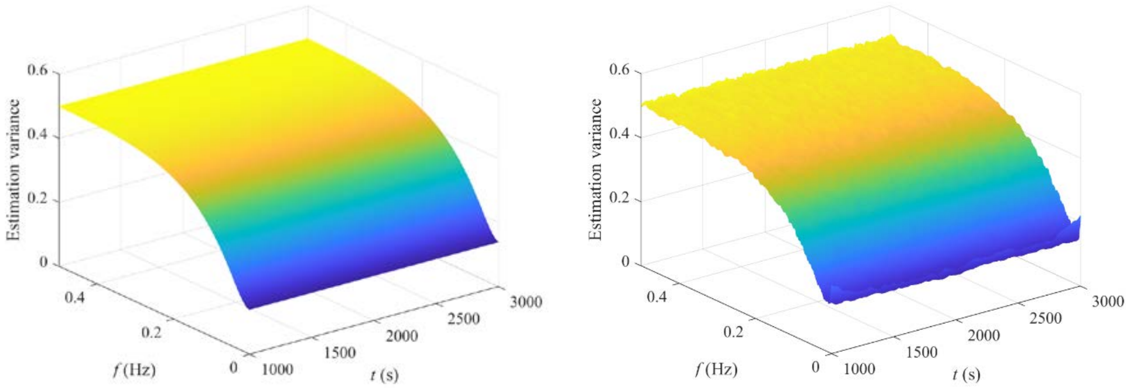

(a) (b)

Fig. 15. Estimation variance of $r_{\mathbf{U}}(t, f)$. (a) the result from Eq. (50) and (b) the result from the 5000 realizations.

In order to verify Theorem 4, a time-invariant coherence is considered, which is obtained by setting $d(t)$ in Eq. (58) as $d(t) = 4\pi$. Then 5000 sets of the realizations of $\mathbf{U}(t)$ with time-invariant coherence are simulated. The estimation bias and variance of the time-invariant coherence are calculated using Eqs. (51) and (53), respectively. The analytical results are compared with those calculated from the 5000 realizations in Fig. 16. It can be seen the analytical bias is consistent with that from the 5000 realizations. The difference between the variance from Eq. (53) and that from the 5000 realizations is not significant.

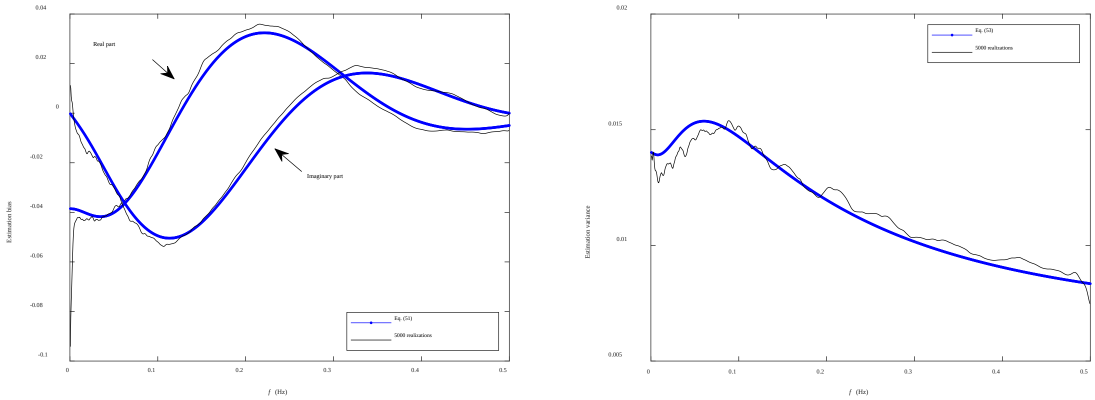

(a) (b)

Fig. 16. Estimation bias and variance of the time-invariant coherence. (a) bias and (b) variance.

6. Real application

Two pieces of ground motion acceleration records TK 3139 and TK 3145, denoted by $a_1(t)$ and $a_2(t)$ in Fig. 17, respectively, were measured from the Mw7.7 Turkey earthquake occurred in Pazarcık (Kahramanmaraş) at 01:17:32AM (UTC+3), 6th Feb. 2023. The east-west direction of the ground motions is adopted. The depth of the earthquake is 8.6 km. The epicenter distance of TK 3139 and TK 3145 is 96.19 km and 91.13 km, respectively. The distance between the two stations is about 6.9 km. The spatial distribution of the epicenter and stations is depicted in Fig. 18. The general information of the earthquake and stations is from AFAD, Turkey.

The WVSes, Loève spectra, and time-invariant and time-varying coherences of $a_1(t)$ and $a_2(t)$ are estimated by the MTST method, in which the first eight $\psi_m(t, f)$, m = 0, 1,…, 7, with a = 0.1, b = 17, and c = 0.4 are utilized. The estimated WVSes, Loève spectra, and coherences are shown in Fig. 19-Fig. 21, respectively. It is illustrated that two WVSes have similar shapes and exhibit obviously non-stationary properties. In the frequency domain, $a_1(t)$ and $a_2(t)$ are correlated in the range of 0 Hz to 1 Hz. The time-varying property of their coherence is not significant. The Loève spectra of $a_1(t)$ and $a_2(t)$ are concentrated near the main diagonal line of the dual-frequency plane with different shapes.

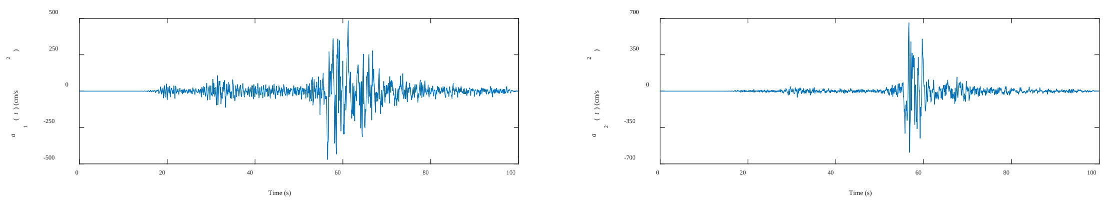

(a) (b)

Fig. 17. The measured ground motion acceleration records. (a) $a_1(t)$ and (b) $a_2(t)$.

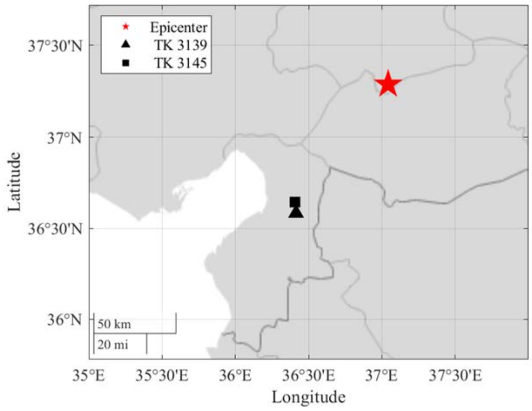

Fig. 18. Spatial distribution of epicenter and two stations for the Feb 2023 Mw7.7 earthquake in Turkey.

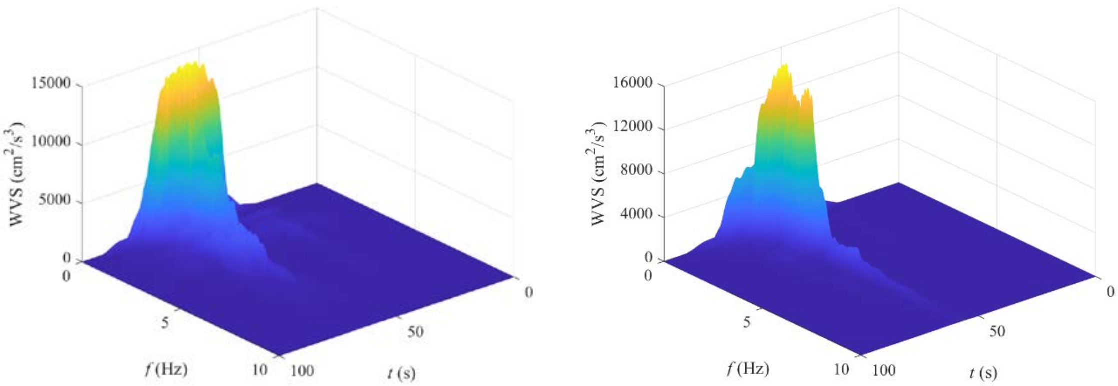

(a) (b)

Fig. 19. The WVSes of $a_1(t)$ and $a_2(t)$. (a) WVS of $a_1(t)$ and (b) WVS of $a_2(t)$.

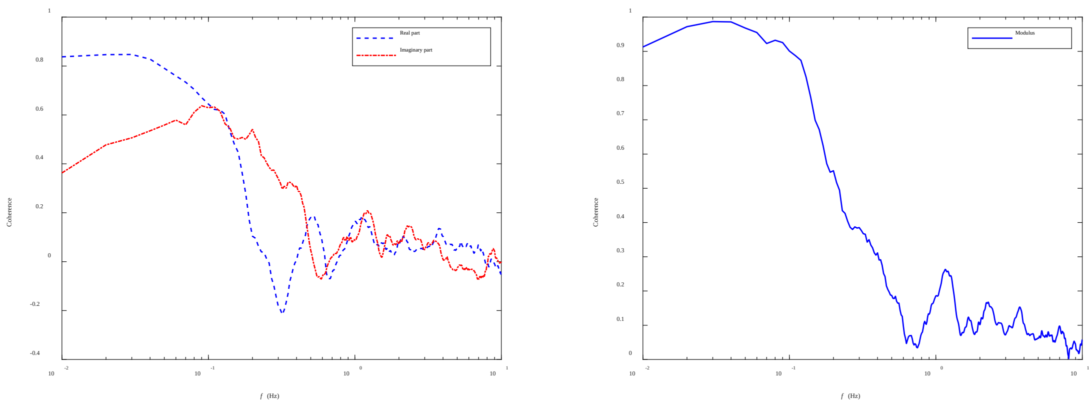

(a) (b)

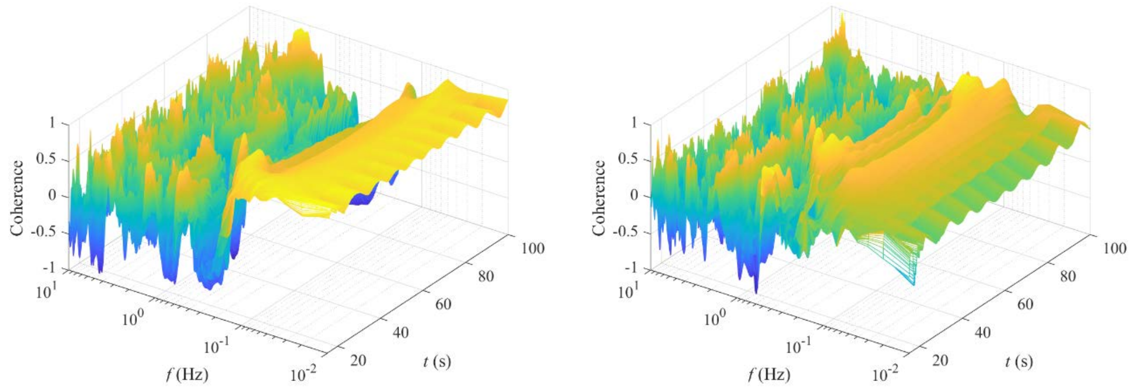

(c) (d)

Fig. 20. Time-invariant and time-varying coherences between $a_1(t)$ and $a_2(t)$. (a) real and imaginary parts of the time-invariant coherence, (b) modulus of the time-invariant coherence, (c) real part of the time-varying coherence, and (d) imaginary part of the time-varying coherence.

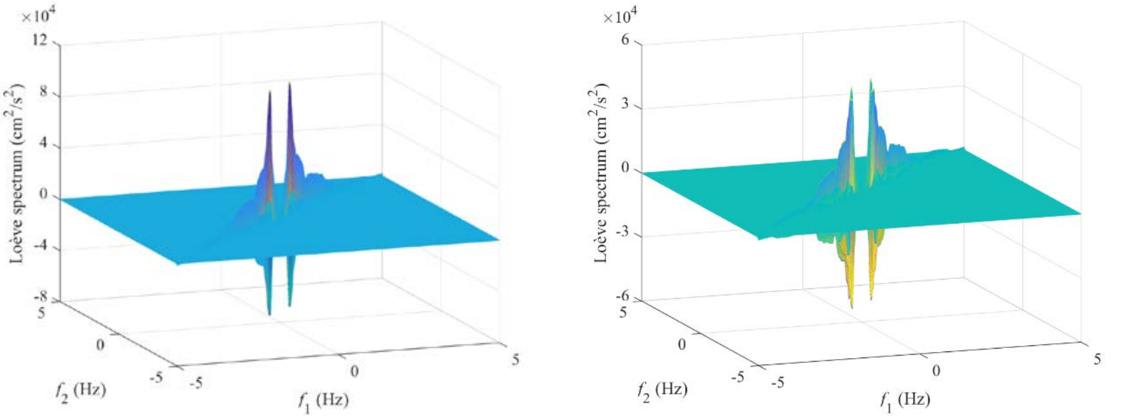

(a) (b)

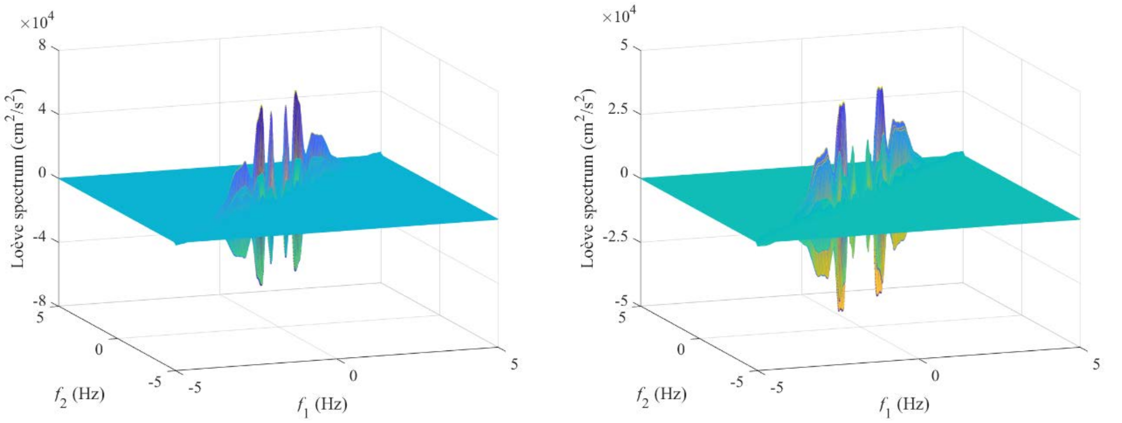

(c) (d)

Fig. 21. Loève spectra of $a_1(t)$ and $a_2(t)$. (a) real part of the Loève spectrum of $a_1(t)$, (b) imaginary part of the Loève spectrum of $a_1(t)$, (c) real part of the Loève spectrum of $a_2(t)$, and (d) imaginary part of the Loève spectrum of $a_2(t)$.

7. Conclusions and prospects

The MTST method for the WVS and Loève spectrum estimations of multi-variate quasi-stationary harmonizable processes is developed in this study. With orthogonal time-frequency Hermite windows, the MTST method can provide sufficient resolutions for the WVS and Loève spectrum estimations and reduce their estimation variances. The biases and variances of the WVS, Loève spectrum, and coherence estimators from the MTST method have also been provided under the assumption that the target multi-variate harmonizable process is Gaussian. The superiority and reliability of the MTST method are verified through comparisons with two multi-taper methods, the Toeplitz kernel method, and the CMS method for the WVS and Loève spectrum estimations using a numerical case of a bivariate harmonizable wind speed process. The results indicate that the MTST method outperforms the existing methods for the WVS and Loève spectrum estimations of quasi-stationary harmonizable processes. Finally, the MTST method is applied to two pieces of ground motion acceleration records measured during the Turkey earthquake in 2023. The two WVSes of the acceleration records have similar shapes and exhibit obviously non-stationary properties. In the frequency domain, the two acceleration records are correlated in the range of 0 Hz to 1 Hz, and the time-varying property of their coherence is not significant. The two acceleration Loève spectra are concentrated near the main diagonal line of the dual-frequency plane with different shapes.

Adaptive determination of the shape parameters a, b, and c in Eq. (14) requires designing a loss function that can optimize the tradeoff between the resolutions along the time and frequency axes. This is a difficult problem and needs further investigation in the future.

CRediT authorship contribution statement

Zifeng Huang: Conceptualization, Methodology, Software, Writing-review & editing; **Guan Chen**: Writing-review & editing, Data curation; **Michael Beer**: Supervision, Project administration.

Declaration of competing interest

The authors declare that they have no known competing financial interests or personal relationships that could have appeared to influence the work reported in this paper.

Data availability statement

The earthquake ground motion acceleration records are from AFAD, Turkey at https://tadas.afad.gov.tr/list-event (last accessed on 28th June 2023). Specifically, two records with station code 3139 and 3145 are selected from the Mw7.7 Turkey earthquake occurred in Pazarcık (Kahramanmaraş) at 01:17:32AM (UTC+3), 6th Feb. 2023.

Acknowledgments

The works described in this paper are financially supported by the Alexander von Humboldt Foundation, to which the authors are most grateful. Any opinions and conclusions presented in this paper are entirely those of the authors.

Appendix A. The proof of Theorem 1

From Eqs. (19) and (28), the estimator $\widehat{\mathbf{W}}(t, f)$ in Eq. (29) can be expressed as

$$\begin{aligned}
&\hat{\mathbf{W}}(t, f) \\
&= \frac{1}{M}\sum_{m=0}^{M-1}\left[\Delta t\sum_{k=-\infty}^{+\infty}\psi_m^*(k\Delta t - t, f)\mathbf{X}^*(k\Delta t)e^{\mathrm{i}2\pi fk\Delta t}\right]\left[\Delta t\sum_{l=-\infty}^{+\infty}\psi_m(l\Delta t - t, f)\mathbf{X}^{\mathrm{T}}(l\Delta t)e^{-\mathrm{i}2\pi fl\Delta t}\right] \\
&= \frac{\Delta t^2}{M}\sum_{m=0}^{M-1}\left[\sum_{k=-\infty}^{+\infty}\sum_{l=-\infty}^{+\infty}\psi_m^*(k\Delta t - t, f)\psi_m(l\Delta t - t, f)\mathbf{X}^*(k\Delta t)\mathbf{X}^{\mathrm{T}}(l\Delta t)e^{\mathrm{i}2\pi f(k-l)\Delta t}\right] \\
&= \Delta t^2\sum_{k=-\infty}^{+\infty}\sum_{l=-\infty}^{+\infty}\left[\frac{1}{M}\sum_{m=0}^{M-1}\psi_m^*(k\Delta t - t, f)\psi_m(l\Delta t - t, f)\right]\mathbf{X}^*(k\Delta t)\mathbf{X}^{\mathrm{T}}(l\Delta t)e^{\mathrm{i}2\pi f(k-l)\Delta t} \\
&= \Delta t^2\sum_{k=-\infty}^{+\infty}\sum_{l=-\infty}^{+\infty}\phi_M(k\Delta t - t, l\Delta t - t, f)\mathbf{X}^*(k\Delta t)\mathbf{X}^{\mathrm{T}}(l\Delta t)e^{\mathrm{i}2\pi f(k-l)\Delta t}.
\end{aligned} \tag{64}$$

From Eq. (64), $\mathrm{E}[\widehat{\mathbf{W}}(t, f)]$ can be expressed as

$$
\begin{aligned}
&\mathrm{E}\left[\hat{\mathbf{W}}(t,f)\right]\\
&=\Delta t^2 \sum_{k=-\infty}^{+\infty}\sum_{l=-\infty}^{+\infty}\phi_M(k\Delta t-t,l\Delta t-t,f)\mathrm{E}\left[\mathbf{X}^*(k\Delta t)\mathbf{X}^{\mathrm{T}}(l\Delta t)\right]e^{\mathrm{i}2\pi f(k-l)\Delta t}\\
&=\Delta t^2 \sum_{k=-\infty}^{+\infty}\sum_{l=-\infty}^{+\infty}\phi_M(k\Delta t-t,l\Delta t-t,f)\mathbf{R}(k\Delta t,l\Delta t)e^{\mathrm{i}2\pi f(k-l)\Delta t}\\
&\overset{(a)}{=}\int_{-\infty}^{+\infty}\int_{-\infty}^{+\infty}\varphi_M(\xi_1,\xi_2,f)e^{\mathrm{i}2\pi(\xi_1-\xi_2)t}\mathbf{S}(f-\xi_1,f-\xi_2)\mathrm{d}\xi_1\mathrm{d}\xi_2\\
&=\int_{-\infty}^{+\infty}\int_{-\infty}^{+\infty}\tilde{\varphi}_M(\xi,\Delta\xi,f)e^{-\mathrm{i}2\pi\Delta\xi t}\mathbf{S}\left[f-(\xi-0.5\Delta\xi),f-(\xi+0.5\Delta\xi)\right]\mathrm{d}\xi\mathrm{d}\Delta\xi\\
&=\int_{-\infty}^{+\infty}\int_{-\infty}^{+\infty}\tilde{\varphi}_M(\xi,\Delta\xi,f)e^{-\mathrm{i}2\pi\Delta\xi t}\tilde{\mathbf{S}}(f-\xi,-\Delta\xi)\mathrm{d}\xi\mathrm{d}\Delta\xi\\
&=\int_{-\infty}^{+\infty}\int_{-\infty}^{+\infty}e^{-\mathrm{i}2\pi\Delta\xi t}\tilde{\varphi}_M(\xi,-\Delta\xi,f)\tilde{\mathbf{S}}(f-\xi,-\Delta\xi)\mathrm{d}\Delta\xi\mathrm{d}\xi\\
&=\int_{-\infty}^{+\infty}\int_{-\infty}^{+\infty}e^{\mathrm{i}2\pi\Delta\xi t}\tilde{\varphi}_M(\xi,\Delta\xi,f)\tilde{\mathbf{S}}(f-\xi,\Delta\xi)\mathrm{d}\Delta\xi\mathrm{d}\xi\\
&\overset{(b)}{=}\int_{-\infty}^{+\infty}\int_{-\infty}^{+\infty}\chi_M(t-\tau,\xi,f)\mathbf{W}(\tau,f-\xi)\mathrm{d}\tau\mathrm{d}\xi\\
&=\int_{-\infty}^{+\infty}\int_{-\infty}^{+\infty}\chi_M(\tau-t,f-\xi,f)\mathbf{W}(\tau,\xi)\mathrm{d}\tau\mathrm{d}\xi,
\end{aligned}
\tag{65}
$$

where (a) and (b) are from the convolution theorem of the Fourier transform. Thus, Bias[$\widehat{\mathbf{W}}(t,f)$] is

$$
\begin{aligned}
\mathrm{Bias}\left[\hat{\mathbf{W}}(t,f)\right]&=\mathrm{E}\left[\hat{\mathbf{W}}(t,f)\right]-\mathbf{W}(t,f)\\
&=\int_{-\infty}^{+\infty}\int_{-\infty}^{+\infty}\chi_M(\tau-t,f-\xi)\mathbf{W}(\tau,\xi)\mathrm{d}\tau\mathrm{d}\xi-\mathbf{W}(t,f)\\
&\overset{(a)}{=}\int_{-\infty}^{+\infty}\int_{-\infty}^{+\infty}\chi_M(\tau-t,f-\xi)\left[\mathbf{W}(\tau,\xi)-\mathbf{W}(t,f)\right]\mathrm{d}\tau\mathrm{d}\xi,
\end{aligned}
\tag{66}
$$

where (a) is from Eq. (27). Eq. (35) can be proved from Eq. (66)

From Eq. (64), the covariance Cov[$\widehat{W}_{ij}(t, f_1)$, $\widehat{W}_{ij}(t, f_2)$] can be calculated as

$$
\begin{aligned}
&\mathrm{Cov}\left[\hat{W}_{ij}(t,f_1),\hat{W}_{ij}(t,f_2)\right]\\
&=\Delta t^4\sum_{k=-\infty}^{+\infty}\sum_{l=-\infty}^{+\infty}\sum_{m=-\infty}^{+\infty}\sum_{n=-\infty}^{+\infty}\left\{e^{\mathrm{i}2\pi f_1(l-k)\Delta t}e^{\mathrm{i}2\pi f_2(m-n)\Delta t}\phi_M^*(k\Delta t-t,l\Delta t-t,f_1)\phi_M(m\Delta t-t,n\Delta t-t,f_2)\right.\\
&\qquad\left.\times\mathrm{Cov}\left[X_i(k\Delta t)X_j^*(l\Delta t),X_i^*(m\Delta t)X_j(n\Delta t)\right]\right\}.
\end{aligned}
\tag{67}
$$

Under the Gaussianity assumption on $\mathbf{X}(t)$, the complex version of the Isserlis' theorem [55, 56] expresses Cov[$X_i(k\Delta t)\,X_j^*(l\Delta t)$, $X_i^*(m\Delta t)\,X_j(n\Delta t)$] as

$$
\begin{aligned}
&\mathrm{Cov}\left[X_i(k\Delta t)X_j^*(l\Delta t),X_i^*(m\Delta t)X_j(n\Delta t)\right]\\
&=\mathrm{E}\left[X_i(k\Delta t)X_i^*(m\Delta t)\right]\mathrm{E}\left[X_j^*(l\Delta t)X_j(n\Delta t)\right]+\mathrm{E}\left[X_i(k\Delta t)X_j(n\Delta t)\right]\mathrm{E}\left[X_j^*(l\Delta t)X_i^*(m\Delta t)\right].
\end{aligned}
\tag{68}
$$

Substituting Eq. (68) into Eq. (67), Cov[$\widehat{W}_{ij}(t, f_1)$, $\widehat{W}_{ij}(t, f_2)$] is calculated as

$$\mathrm{Cov}\left[\hat{W}_{ij}(t, f_1), \hat{W}_{ij}(t, f_2)\right] = C_1(t, f_1, f_2) + C_2(t, f_1, f_2), \tag{69}$$

where

$$\begin{aligned}
&C_1(t, f_1, f_2)\\
&= \Delta t^4 \sum_{k=-\infty}^{+\infty}\sum_{l=-\infty}^{+\infty}\sum_{m=-\infty}^{+\infty}\sum_{n=-\infty}^{+\infty}\Big\{e^{\mathrm{i}2\pi f_1(l-k)\Delta t}e^{\mathrm{i}2\pi f_2(m-n)\Delta t}\phi_M^*(k\Delta t - t, l\Delta t - t, f_1)\phi_M(m\Delta t - t, n\Delta t - t, f_2)\\
&\quad\times \mathrm{E}\left[X_i(k\Delta t)X_i^*(m\Delta t)\right]\mathrm{E}\left[X_j^*(l\Delta t)X_j(n\Delta t)\right]\Big\}\\
&= \Delta t^4 \sum_{k=-\infty}^{+\infty}\sum_{l=-\infty}^{+\infty}\sum_{m=-\infty}^{+\infty}\sum_{n=-\infty}^{+\infty}\Big\{e^{\mathrm{i}2\pi f_1(l-k)\Delta t}e^{\mathrm{i}2\pi f_2(m-n)\Delta t}\phi_M^*(k\Delta t - t, l\Delta t - t, f_1)\phi_M(m\Delta t - t, n\Delta t - t, f_2)\\
&\quad\times R_{ii}^*(k\Delta t, m\Delta t)R_{jj}(l\Delta t, n\Delta t)\Big\},
\end{aligned} \tag{70}$$

$$\begin{aligned}
&C_2(t, f_1, f_2)\\
&= \Delta t^4 \sum_{k=-\infty}^{+\infty}\sum_{l=-\infty}^{+\infty}\sum_{m=-\infty}^{+\infty}\sum_{n=-\infty}^{+\infty}\Big\{e^{\mathrm{i}2\pi f_1(l-k)\Delta t}e^{\mathrm{i}2\pi f_2(m-n)\Delta t}\phi_M^*(k\Delta t - t, l\Delta t - t, f_1)\phi_M(m\Delta t - t, n\Delta t - t, f_2)\\
&\quad\times \mathrm{E}\left[X_i(k\Delta t)X_j(n\Delta t)\right]\mathrm{E}\left[X_j^*(l\Delta t)X_i^*(m\Delta t)\right]\Big\}\\
&= \Delta t^4 \sum_{k=-\infty}^{+\infty}\sum_{l=-\infty}^{+\infty}\sum_{m=-\infty}^{+\infty}\sum_{n=-\infty}^{+\infty}\Big\{e^{\mathrm{i}2\pi f_1(l-k)\Delta t}e^{\mathrm{i}2\pi f_2(m-n)\Delta t}\phi_M^*(k\Delta t - t, l\Delta t - t, f_1)\phi_M(m\Delta t - t, n\Delta t - t, f_2)\\
&\quad\times \mathrm{E}\left[X_i(k\Delta t)X_j^*(n\Delta t)\right]\mathrm{E}\left[X_i^*(m\Delta t)X_j(l\Delta t)\right]\Big\}\\
&= \Delta t^4 \sum_{k=-\infty}^{+\infty}\sum_{l=-\infty}^{+\infty}\sum_{m=-\infty}^{+\infty}\sum_{n=-\infty}^{+\infty}\Big\{e^{\mathrm{i}2\pi f_1(l-k)\Delta t}e^{\mathrm{i}2\pi f_2(m-n)\Delta t}\phi_M^*(k\Delta t - t, l\Delta t - t, f_1)\phi_M(m\Delta t - t, n\Delta t - t, f_2)\\
&\quad\times R_{ij}^*(k\Delta t, n\Delta t)R_{ij}(m\Delta t, l\Delta t)\Big\}
\end{aligned} \tag{71}$$

and $R_{ij}(t_1, t_2)$ is the ij^{th} element of $\mathbf{R}(t_1, t_2)$ in Eq. (5).

Assuming that $\mathbf{X}(t)$ is quasi-stationary in the valid range of window $\phi_M(t_1, t_2)$ [22], then the four correlations in Eqs. (70) and (71) are approximated by

$$r_{ij,t}(\tau) = R_{ij}(t - 0.5\tau, t + 0.5\tau) = \int_{-\infty}^{+\infty} e^{\mathrm{i}2\pi f\tau}W_{ij}(t, f)\mathrm{d}f. \tag{72}$$

Substituting Eq. (72) into Eqs. (70) and (71), $C_1(t, f_1, f_2)$ and $C_2(t, f_1, f_2)$ can be respectively approximated as

$$\begin{aligned}
&C_1(t, f_1, f_2)\\
&\approx \Delta t^4 \sum_{k=-\infty}^{+\infty}\sum_{l=-\infty}^{+\infty}\sum_{m=-\infty}^{+\infty}\sum_{n=-\infty}^{+\infty}\Big\{e^{\mathrm{i}2\pi f_1(l-k)\Delta t}e^{\mathrm{i}2\pi f_2(m-n)\Delta t}\phi_M^*(k\Delta t, l\Delta t, f_1)\phi_M(m\Delta, n\Delta t, f_2)\\
&\quad\times r_{ii,t}^*\left[(m-k)\Delta t\right]r_{jj,t}\left[(n-l)\Delta t\right]\Big\}
\end{aligned} \tag{73}$$

and

$$
\begin{aligned}
&C_2(t, f_1, f_2) \\
&\approx \Delta t^4 \sum_{k=-\infty}^{+\infty}\sum_{l=-\infty}^{+\infty}\sum_{m=-\infty}^{+\infty}\sum_{n=-\infty}^{+\infty}\left\{e^{\mathrm{i}2\pi f_1(l-k)\Delta t}e^{\mathrm{i}2\pi f_2(m-n)\Delta t}\phi_M^*(k\Delta t, l\Delta t, f_1)\phi_M(m\Delta t, n\Delta t, f_2)\right. \\
&\quad \left.\times r_{ij,t}^*\left[(n-k)\Delta t\right]r_{ij,t}\left[(l-m)\Delta t\right]\right\}.
\end{aligned}
\tag{74}
$$

Further $C_1(t, f_1, f_2)$ is

$$
\begin{aligned}
&C_1(t, f_1, f_2) \\
&\approx \Delta t^4 \sum_{k=-\infty}^{+\infty}\sum_{l=-\infty}^{+\infty}\sum_{m=-\infty}^{+\infty}\sum_{n=-\infty}^{+\infty}\left\{e^{\mathrm{i}2\pi f_1(l-k)\Delta t}e^{\mathrm{i}2\pi f_2(m-n)\Delta t}\phi_M^*(k\Delta t, l\Delta t, f_1)\phi_M(m\Delta t, n\Delta t, f_2)\right. \\
&\quad \left.\times\int_{-\infty}^{+\infty}e^{-\mathrm{i}2\pi\xi(m-k)\Delta t}W_{ii}^*(t,\xi)\mathrm{d}\xi\int_{-\infty}^{+\infty}e^{\mathrm{i}2\pi\lambda(n-l)\Delta t}W_{jj}(t,\lambda)\mathrm{d}\lambda\right\} \\
&\approx \Delta t^4\int_{-\infty}^{+\infty}\int_{-\infty}^{+\infty}\left\{\sum_{k=-\infty}^{+\infty}\sum_{l=-\infty}^{+\infty}\sum_{m=-\infty}^{+\infty}\sum_{n=-\infty}^{+\infty}e^{\mathrm{i}2\pi f_1(l-k)\Delta t}e^{\mathrm{i}2\pi f_2(m-n)\Delta t}e^{\mathrm{i}2\pi\xi(k-m)\Delta t}e^{\mathrm{i}2\pi\lambda(n-l)\Delta t}\right. \\
&\qquad \left.\times\phi_M^*(k\Delta t, l\Delta t, f_1)\phi_M(m\Delta t, n\Delta t, f_2)W_{ii}^*(t,\xi)W_{jj}(t,\lambda)\right\}\mathrm{d}\xi\mathrm{d}\lambda \\
&\approx \Delta t^4\int_{-\infty}^{+\infty}\int_{-\infty}^{+\infty}\left\{\sum_{k=-\infty}^{+\infty}\sum_{l=-\infty}^{+\infty}\sum_{m=-\infty}^{+\infty}\sum_{n=-\infty}^{+\infty}e^{\mathrm{i}2\pi(\xi-f_1)k\Delta t}e^{\mathrm{i}2\pi(f_1-\lambda)l\Delta t}e^{\mathrm{i}2\pi(f_2-\xi)m\Delta t}e^{\mathrm{i}2\pi(\lambda-f_2)n\Delta t}\right. \\
&\qquad \left.\times\phi_M^*(k\Delta t, l\Delta t, f_1)\phi_M(m\Delta t, n\Delta t, f_2)W_{ii}^*(t,\xi)W_{jj}(t,\lambda)\right\}\mathrm{d}\xi\mathrm{d}\lambda \\
&\approx \int_{-\infty}^{+\infty}\int_{-\infty}^{+\infty}\left\{\Delta t^2\sum_{k=-\infty}^{+\infty}\sum_{l=-\infty}^{+\infty}e^{-\mathrm{i}2\pi(f_1-\xi)k\Delta t}e^{\mathrm{i}2\pi(f_1-\lambda)l\Delta t}\phi_M^*(k\Delta t, l\Delta t, f_1)\right. \\
&\qquad \left.\times\Delta t^2\sum_{m=-\infty}^{+\infty}\sum_{n=-\infty}^{+\infty}e^{\mathrm{i}2\pi(f_2-\xi)m\Delta t}e^{-\mathrm{i}2\pi(f_2-\lambda)n\Delta t}\phi_M(m\Delta t, n\Delta t, f_2)W_{ii}^*(t,\xi)W_{jj}(t,\lambda)\right\}\mathrm{d}\xi\mathrm{d}\lambda \\
&\approx \int_{-\infty}^{+\infty}\int_{-\infty}^{+\infty}\varphi_M^*(f_1-\xi, f_1-\lambda, f_1)\varphi_M(f_2-\xi, f_2-\lambda, f_2)W_{ii}^*(t,\xi)W_{jj}(t,\lambda)\mathrm{d}\xi\mathrm{d}\lambda \\
&\approx \int_{-\infty}^{+\infty}\int_{-\infty}^{+\infty}\tilde{\varphi}_M^*\left[f_1-0.5(\xi+\lambda),\xi-\lambda, f_1\right]\tilde{\varphi}_M\left[f_2-0.5(\xi+\lambda),\xi-\lambda, f_2\right]W_{ii}^*(t,\xi)W_{jj}(t,\lambda)\mathrm{d}\xi\mathrm{d}\lambda \\
&\approx \int_{-\infty}^{+\infty}\int_{-\infty}^{+\infty}\tilde{\varphi}_M^*(f_1-u,-v, f_1)\tilde{\varphi}_M(f_2-u,-v, f_2)W_{ii}^*(t,u-0.5v)W_{jj}(t,u+0.5v)\mathrm{d}u\mathrm{d}v \\
&\approx \int_{-\infty}^{+\infty}\int_{-\infty}^{+\infty}\tilde{\varphi}_M^*(f_1-u,v, f_1)\tilde{\varphi}_M(f_2-u,v, f_2)W_{ii}^*(t,u-0.5v)W_{jj}(t,u+0.5v)\mathrm{d}u\mathrm{d}v.
\end{aligned}
\tag{75}
$$

Then $C_1(t, f, f)$ is approximated as

$$
C_1(t, f, f) \approx \int_{-\infty}^{+\infty}\int_{-\infty}^{+\infty}\tilde{\varphi}_M^*(u-f, v, f)\tilde{\varphi}_M(u-f, v, f)W_{ii}^*(t,u-0.5v)W_{jj}(t,u+0.5v)\mathrm{d}u\mathrm{d}v. \tag{76}
$$

$C_2(t, f_1, f_2)$ in Eq. (74) can be further calculated as

$$
\begin{aligned}
&C_2(t, f_1, f_2) \\
&\approx \Delta t^4 \sum_{k=-\infty}^{+\infty}\sum_{l=-\infty}^{+\infty}\sum_{m=-\infty}^{+\infty}\sum_{n=-\infty}^{+\infty}\Big\{ e^{\mathrm{i}2\pi f_1(l-k)\Delta t} e^{\mathrm{i}2\pi f_2(m-n)\Delta t} \phi_M^*(k\Delta t, l\Delta t, f_1)\phi_M(m\Delta t, n\Delta t, f_2) \\
&\quad \times \int_{-\infty}^{+\infty} e^{-\mathrm{i}2\pi\xi(n-k)\Delta t} W_{ij}^*(t,\xi)\mathrm{d}\xi \int_{-\infty}^{+\infty} e^{\mathrm{i}2\pi\lambda(l-m)\Delta t} W_{ij}(t,\lambda)\mathrm{d}\lambda \Big\} \\
&\approx \Delta t^4 \int_{-\infty}^{+\infty}\int_{-\infty}^{+\infty}\Big\{ \sum_{k=-\infty}^{+\infty}\sum_{l=-\infty}^{+\infty}\sum_{m=-\infty}^{+\infty}\sum_{n=-\infty}^{+\infty} e^{-\mathrm{i}2\pi\xi(n-k)\Delta t} e^{\mathrm{i}2\pi\lambda(l-m)\Delta t} e^{\mathrm{i}2\pi f_1(l-k)\Delta t} e^{\mathrm{i}2\pi f_2(m-n)\Delta t} \\
&\qquad\qquad \times \phi_M^*(k\Delta t, l\Delta t, f_1)\phi_M(m\Delta t, n\Delta t, f_2) W_{ij}^*(t,\xi) W_{ij}(t,\lambda)\Big\}\mathrm{d}\xi\mathrm{d}\lambda \\
&\approx \Delta t^4 \int_{-\infty}^{+\infty}\int_{-\infty}^{+\infty}\Big\{ \sum_{k=-\infty}^{+\infty}\sum_{l=-\infty}^{+\infty}\sum_{m=-\infty}^{+\infty}\sum_{n=-\infty}^{+\infty} e^{\mathrm{i}2\pi(\xi-f_1)k\Delta t} e^{\mathrm{i}2\pi(\lambda+f_1)l\Delta t} e^{\mathrm{i}2\pi(f_2-\lambda)m\Delta t} e^{-\mathrm{i}2\pi(\xi+f_2)n\Delta t} \\
&\qquad\qquad \times \phi_M^*(k\Delta t, l\Delta t, f_1)\phi_M(m\Delta t, n\Delta t, f_2) W_{ij}^*(t,\xi) W_{ij}(t,\lambda)\Big\}\mathrm{d}\xi\mathrm{d}\lambda \\
&\approx \int_{-\infty}^{+\infty}\int_{-\infty}^{+\infty}\Big\{ \Delta t^2 \sum_{k=-\infty}^{+\infty}\sum_{l=-\infty}^{+\infty} e^{-\mathrm{i}2\pi(f_1-\xi)k\Delta t} e^{\mathrm{i}2\pi(\lambda+f_1)l\Delta t} \phi_M^*(k\Delta t, l\Delta t, f_1) \\
&\qquad \times \Delta t^2 \sum_{m=-\infty}^{+\infty}\sum_{n=-\infty}^{+\infty} e^{\mathrm{i}2\pi(f_2-\lambda)m\Delta t} e^{-\mathrm{i}2\pi(\xi+f_2)n\Delta t} \phi_M(m\Delta t, n\Delta t, f_2) W_{ij}^*(t,\xi) W_{ij}(t,\lambda)\Big\}\mathrm{d}\xi\mathrm{d}\lambda \\
&\approx \int_{-\infty}^{+\infty}\int_{-\infty}^{+\infty} \varphi_M^*(f_1-\xi, \lambda+f_1, f_1)\varphi_M(f_2-\lambda, \xi+f_2, f_2) W_{ij}^*(t,\xi) W_{ij}(t,\lambda)\mathrm{d}\xi\mathrm{d}\lambda \\
&\approx \int_{-\infty}^{+\infty}\int_{-\infty}^{+\infty} \tilde{\varphi}_M^*\left[f_1+0.5(\lambda-\xi), \xi+\lambda, f_1\right]\tilde{\varphi}_M\left[f_2+0.5(\xi-\lambda), \xi+\lambda, f_2\right] W_{ij}^*(t,\xi) W_{ij}(t,\lambda)\mathrm{d}\xi\mathrm{d}\lambda \\
&\approx \int_{-\infty}^{+\infty}\int_{-\infty}^{+\infty} \tilde{\varphi}_M^*(f_1+0.5v, 2u, f_1)\tilde{\varphi}_M(f_2-0.5v, 2u, f_2) W_{ij}^*(t, u-0.5v) W_{ij}(t, u+0.5v)\mathrm{d}u\mathrm{d}v,
\end{aligned} \tag{77}
$$

Then $C_2(t, f, f)$ is approximated as

$$
C_2(t, f, f) \approx \int_{-\infty}^{+\infty}\int_{-\infty}^{+\infty} \tilde{\varphi}_M^*(f+0.5v, 2u, f)\tilde{\varphi}_M(f-0.5v, 2u, f) W_{ij}^*(t, u-0.5v) W_{ij}(t, u+0.5v)\mathrm{d}u\mathrm{d}v. \tag{78}
$$

From Eqs. (69), (76) and (78), Eq. (36) is proved.

Appendix B. The proof of Corollary 1

With the conditions in Theorem 1, and $\tilde{\varphi}_M(u, v, f)$ is more concentrated compared with $W_{ii}(t, u + 0.5v)$, $W_{jj}(t, u + 0.5v)$ and $W_{ij}(t, u + 0.5v)$, then $\mathrm{Var}[\widehat{W}_{ij}(t, f)]$ in Eq. (36) can be approximately simplified

$$
\begin{aligned}
&\mathrm{Var}\left[\hat{W}_{ij}(t,f)\right]\\
&\approx \int_{-\infty}^{+\infty}\int_{-\infty}^{+\infty}\tilde{\varphi}_M^*(u-f,v,f)\tilde{\varphi}_M(u-f,v,f)W_{ii}^*(t,u)W_{jj}(t,u)\mathrm{d}u\mathrm{d}v\\
&\quad+\int_{-\infty}^{+\infty}\int_{-\infty}^{+\infty}\tilde{\varphi}_M^*(f+0.5v,2u,f)\tilde{\varphi}_M(f-0.5v,2u,f)W_{ij}^*(t,-0.5v)W_{ij}(t,0.5v)\mathrm{d}u\mathrm{d}v\\
&\approx W_{ii}^*(t,f)W_{jj}(t,f)\int_{-\infty}^{+\infty}\int_{-\infty}^{+\infty}\left|\tilde{\varphi}_M(u,v,f)\right|^2\mathrm{d}u\mathrm{d}v\\
&\quad+\left|W_{ij}(t,f)\right|^2\int_{-\infty}^{+\infty}\int_{-\infty}^{+\infty}\tilde{\varphi}_M^*(f+0.5v,2u,f)\tilde{\varphi}_M(f-0.5v,2u,f)\mathrm{d}u\mathrm{d}v\\
&\approx W_{ii}^*(t,f)W_{jj}(t,f)\int_{-\infty}^{+\infty}\int_{-\infty}^{+\infty}\left|\tilde{\varphi}_M(u,v,f)\right|^2\mathrm{d}u\mathrm{d}v\\
&\quad+\left|W_{ij}(t,f)\right|^2\int_{-\infty}^{+\infty}\int_{-\infty}^{+\infty}\tilde{\varphi}_M^*(f+v,u,f)\tilde{\varphi}_M(f-v,u,f)\mathrm{d}u\mathrm{d}v,
\end{aligned}
\tag{79}
$$

where

$$
\begin{aligned}
&\int_{-\infty}^{+\infty}\int_{-\infty}^{+\infty}\left|\tilde{\varphi}_M(u,v,f)\right|^2\mathrm{d}u\mathrm{d}v\\
&=\int_{-\infty}^{+\infty}\int_{-\infty}^{+\infty}\left|\varphi_M(f_1,f_2,f)\right|^2\mathrm{d}f_1\mathrm{d}f_2\\
&=\Delta t^2\sum_{k=-\infty}^{+\infty}\sum_{l=-\infty}^{+\infty}\left|\phi_M(k\Delta t,l\Delta t,f)\right|^2\\
&=\Delta t^2\sum_{k=-\infty}^{+\infty}\sum_{l=-\infty}^{+\infty}\left|\frac{1}{M}\sum_{m=0}^{M-1}\psi_m^*(k\Delta t,f)\psi_m(l\Delta t,f)\right|^2\\
&=\frac{\Delta t^2}{M^2}\sum_{k=-\infty}^{+\infty}\sum_{l=-\infty}^{+\infty}\sum_{m=0}^{M-1}\sum_{n=0}^{M-1}\psi_m(k\Delta t,f)\psi_m^*(l\Delta t,f)\psi_n^*(k\Delta t,f)\psi_n(l\Delta t,f)\\
&=\frac{1}{M^2}\sum_{m=0}^{M-1}\sum_{n=0}^{M-1}\left[\Delta t^2\sum_{k=-\infty}^{+\infty}\sum_{l=-\infty}^{+\infty}\psi_m(k\Delta t,f)\psi_m^*(l\Delta t,f)\psi_n^*(k\Delta t,f)\psi_n(l\Delta t,f)\right]\\
&=\frac{1}{M^2}\sum_{m=0}^{M-1}\sum_{n=0}^{M-1}\left[\Delta t\sum_{k=-\infty}^{+\infty}\psi_m(k\Delta t,f)\psi_n^*(k\Delta t,f)\right]\left[\Delta t\sum_{l=-\infty}^{+\infty}\psi_m^*(l\Delta t,f)\psi_n(l\Delta t,f)\right]\\
&=\frac{1}{M^2}\sum_{m=0}^{M-1}\sum_{n=0}^{M-1}\delta_{mn}\delta_{mn}\\
&=\frac{1}{M}.
\end{aligned}
\tag{80}
$$

Substituting Eq. (80) into Eq. (79), Eq. (37) is proved.

Appendix C. The proof of Theorem 2

Substituting Eq. (64) into Eq. (30), $\hat{\mathbf{S}}(f_1,\ f_2)$ can be expressed as

$$
\begin{aligned}
&\hat{\mathbf{S}}(f_1, f_2) \\
&= \Delta t \sum_{k=-\lceil L[0.5(f_1+f_2)]/2 \rceil+1}^{\lfloor L[0.5(f_1+f_2)]/2 \rfloor} \Big\{ e^{-\mathrm{i}2\pi(f_2-f_1)k\Delta t} \\
&\quad \times \Delta t^2 \sum_{m=-\infty}^{+\infty} \sum_{n=-\infty}^{+\infty} \phi_M\left[(m-k)\Delta t,(n-k)\Delta t,0.5(f_1+f_2)\right]\mathbf{X}^*(m\Delta t)\mathbf{X}^{\mathrm{T}}(n\Delta t)e^{\mathrm{i}2\pi[0.5(f_1+f_2)](m-n)\Delta t} \Big\} \\
&= \Delta t \sum_{k=-\infty}^{+\infty} \Big\{ \Pi\left[k\Delta t, 0.5(f_1+f_2)\right] e^{-\mathrm{i}2\pi(f_2-f_1)k\Delta t} \\
&\quad \times \Delta t^2 \sum_{m=-\infty}^{+\infty} \sum_{n=-\infty}^{+\infty} \phi_M\left[(m-k)\Delta t,(n-k)\Delta t,0.5(f_1+f_2)\right]\mathbf{X}^*(m\Delta t)\mathbf{X}^{\mathrm{T}}(n\Delta t)e^{\mathrm{i}2\pi[0.5(f_1+f_2)](m-n)\Delta t} \Big\},
\end{aligned}
\tag{81}
$$

where $\Pi(t, f)$ in defined in Eq. (40),

$$
\phi_M\left[(m-k)\Delta t,(n-k)\Delta t,0.5(f_1+f_2)\right] = \int_{-\infty}^{+\infty}\int_{-\infty}^{+\infty} e^{\mathrm{i}2\pi[\lambda_2(n-k)-\lambda_1(m-k)]\Delta t}\varphi_M\left[\lambda_1,\lambda_2,0.5(f_1+f_2)\right]\mathrm{d}\lambda_1\mathrm{d}\lambda_2 \tag{82}
$$

and

$$
\mathbf{X}^*(m\Delta t)\mathbf{X}^{\mathrm{T}}(n\Delta t) = \int_{-\infty}^{+\infty}\int_{-\infty}^{+\infty} e^{\mathrm{i}2\pi(\xi_2 n-\xi_1 m)\Delta t}\mathrm{d}\mathbf{Z}^*(\xi_1)\mathrm{d}\mathbf{Z}^{\mathrm{T}}(\xi_2). \tag{83}
$$

Using Eqs. (82) and (83), the second term on the right side of Eq. (81) can be expressed as

$$
\begin{aligned}
&\Delta t^2 \sum_{m=-\infty}^{+\infty} \sum_{n=-\infty}^{+\infty} \phi_M\left[(m-k)\Delta t,(n-k)\Delta t,0.5(f_1+f_2)\right]\mathbf{X}^*(m\Delta t)\mathbf{X}^{\mathrm{T}}(n\Delta t)e^{\mathrm{i}2\pi[0.5(f_1+f_2)](m-n)\Delta t} \\
&= \Delta t^2 \sum_{m=-\infty}^{+\infty} \sum_{n=-\infty}^{+\infty} \Big\{ e^{\mathrm{i}2\pi[0.5(f_1+f_2)](m-n)\Delta t} \int_{-\infty}^{+\infty}\int_{-\infty}^{+\infty} e^{\mathrm{i}2\pi[\lambda_2(n-k)-\lambda_1(m-k)]\Delta t}\varphi_M\left[\lambda_1,\lambda_2,0.5(f_1+f_2)\right]\mathrm{d}\lambda_1\mathrm{d}\lambda_2 \\
&\qquad\qquad \times \int_{-\infty}^{+\infty}\int_{-\infty}^{+\infty} e^{\mathrm{i}2\pi(\xi_2 n-\xi_1 m)\Delta t}\mathrm{d}\mathbf{Z}^*(\xi_1)\mathrm{d}\mathbf{Z}^{\mathrm{T}}(\xi_2) \Big\} \\
&= \int_{-\infty}^{+\infty}\int_{-\infty}^{+\infty}\int_{-\infty}^{+\infty}\int_{-\infty}^{+\infty} \varphi_M\left[\lambda_1,\lambda_2,0.5(f_1+f_2)\right] \\
&\quad \times \left\{ \Delta t^2 \sum_{m=-\infty}^{+\infty} \sum_{n=-\infty}^{+\infty} e^{\mathrm{i}2\pi[0.5(f_1+f_2)](m-n)\Delta t} e^{\mathrm{i}2\pi[\lambda_2(n-k)-\lambda_1(m-k)]\Delta t} e^{\mathrm{i}2\pi(\xi_2 n-\xi_1 m)\Delta t} \right\} \mathrm{d}\lambda_1\mathrm{d}\lambda_2\mathrm{d}\mathbf{Z}^*(\xi_1)\mathrm{d}\mathbf{Z}^{\mathrm{T}}(\xi_2) \\
&= \int_{-\infty}^{+\infty}\int_{-\infty}^{+\infty}\int_{-\infty}^{+\infty}\int_{-\infty}^{+\infty} e^{\mathrm{i}2\pi(\lambda_1-\lambda_2)k\Delta t}\varphi_M\left[\lambda_1,\lambda_2,0.5(f_1+f_2)\right] \\
&\quad \times \left\{ \Delta t \sum_{m=-\infty}^{+\infty} e^{\mathrm{i}2\pi[0.5(f_1+f_2)-\lambda_1-\xi_1]m\Delta t} \Delta t \sum_{n=-\infty}^{+\infty} e^{-\mathrm{i}2\pi[0.5(f_1+f_2)-\lambda_2-\xi_2]n\Delta t} \right\} \mathrm{d}\lambda_1\mathrm{d}\lambda_2\mathrm{d}\mathbf{Z}^*(\xi_1)\mathrm{d}\mathbf{Z}^{\mathrm{T}}(\xi_2) \\
&\overset{(a)}{=} \int_{-\infty}^{+\infty}\int_{-\infty}^{+\infty}\int_{-\infty}^{+\infty}\int_{-\infty}^{+\infty} e^{\mathrm{i}2\pi(\lambda_1-\lambda_2)k\Delta t}\varphi_M\left[\lambda_1,\lambda_2,0.5(f_1+f_2)\right] \\
&\quad \times \left\{ \delta\left[0.5(f_1+f_2)-\lambda_1-\xi_1\right]\delta\left[0.5(f_1+f_2)-\lambda_2-\xi_2\right] \right\} \mathrm{d}\lambda_1\mathrm{d}\lambda_2\mathrm{d}\mathbf{Z}^*(\xi_1)\mathrm{d}\mathbf{Z}^{\mathrm{T}}(\xi_2) \\
&= \int_{-\infty}^{+\infty}\int_{-\infty}^{+\infty} e^{\mathrm{i}2\pi(\xi_2-\xi_1)k\Delta t}\varphi_M\left[0.5(f_1+f_2)-\xi_1, 0.5(f_1+f_2)-\xi_2, 0.5(f_1+f_2)\right]\mathrm{d}\mathbf{Z}^*(\xi_1)\mathrm{d}\mathbf{Z}^{\mathrm{T}}(\xi_2),
\end{aligned}
\tag{84}
$$

where (a) is from the fact that $\varphi_M(f_1, f_2, f)$ only has values in the range of $(f_1, f_2) \in [-f_{\mathrm{N}}, f_{\mathrm{N}}]^2$ indicated in Eq. (22) and $\delta(\bullet)$ is the Dirac delta function. Substituting Eq. (84) into Eq. (81), $\hat{\mathbf{S}}(f_1, f_2)$ is expressed as

$$
\begin{aligned}
&\hat{\mathbf{S}}(f_1, f_2)\\
&= \Delta t \sum_{k=-\infty}^{+\infty} \Big\{ \Pi\left[k\Delta t, 0.5(f_1+f_2)\right] e^{-\mathrm{i}2\pi(f_2-f_1)k\Delta t}\\
&\quad \times \int_{-\infty}^{+\infty}\int_{-\infty}^{+\infty} e^{\mathrm{i}2\pi(\xi_2-\xi_1)k\Delta t} \varphi_M\left[0.5(f_1+f_2)-\xi_1, 0.5(f_1+f_2)-\xi_2, 0.5(f_1+f_2)\right] \mathrm{d}\mathbf{Z}^*(\xi_1)\mathrm{d}\mathbf{Z}^{\mathrm{T}}(\xi_2) \Big\}\\
&= \int_{-\infty}^{+\infty}\int_{-\infty}^{+\infty} \left\{ \Delta t \sum_{k=-\infty}^{+\infty} \Pi\left[k\Delta t, 0.5(f_1+f_2)\right] e^{-\mathrm{i}2\pi(f_2-f_1)k\Delta t} e^{\mathrm{i}2\pi(\xi_2-\xi_1)k\Delta t} \right\}\\
&\quad \times \varphi_M\left[0.5(f_1+f_2)-\xi_1, 0.5(f_1+f_2)-\xi_2, 0.5(f_1+f_2)\right] \mathrm{d}\mathbf{Z}^*(\xi_1)\mathrm{d}\mathbf{Z}^{\mathrm{T}}(\xi_2) \qquad (85)\\
&= \int_{-\infty}^{+\infty}\int_{-\infty}^{+\infty} \left\{ \Delta t \sum_{k=-\infty}^{+\infty} \Pi\left[k\Delta t, 0.5(f_1+f_2)\right] e^{-\mathrm{i}2\pi[(f_2-f_1)-(\xi_2-\xi_1)]k\Delta t} \right\}\\
&\quad \times \varphi_M\left[0.5(f_1+f_2)-\xi_1, 0.5(f_1+f_2)-\xi_2, 0.5(f_1+f_2)\right] \mathrm{d}\mathbf{Z}^*(\xi_1)\mathrm{d}\mathbf{Z}^{\mathrm{T}}(\xi_2)\\
&= \int_{-\infty}^{+\infty}\int_{-\infty}^{+\infty} F_\Pi\left[(f_2-f_1)-(\xi_2-\xi_1), 0.5(f_1+f_2)\right]\\
&\quad \times \varphi_M\left[0.5(f_1+f_2)-\xi_1, 0.5(f_1+f_2)-\xi_2, 0.5(f_1+f_2)\right] \mathrm{d}\mathbf{Z}^*(\xi_1)\mathrm{d}\mathbf{Z}^{\mathrm{T}}(\xi_2),
\end{aligned}
$$

where $F_\Pi(\lambda, f)$ is in Eq. (39). The expectation $\mathrm{E}[\hat{\mathbf{S}}(f_1, f_2)]$ of $\hat{\mathbf{S}}(f_1, f_2)$ in Eq. (30) is calculated as

$$
\begin{aligned}
&\mathrm{E}\left[\hat{\mathbf{S}}(f_1, f_2)\right]\\
&= \int_{-\infty}^{+\infty}\int_{-\infty}^{+\infty} F_\Pi\left[(f_2-f_1)-(\xi_2-\xi_1), 0.5(f_1+f_2)\right]\\
&\quad \times \varphi_M\left[0.5(f_1+f_2)-\xi_1, 0.5(f_1+f_2)-\xi_2, 0.5(f_1+f_2)\right] \mathbf{S}(\xi_1,\xi_2)\mathrm{d}\xi_1\mathrm{d}\xi_2 \qquad (86)\\
&= \int_{-\infty}^{+\infty}\int_{-\infty}^{+\infty} F_\Pi\left[(f_2-f_1)-\lambda, 0.5(f_1+f_2)\right] \tilde{\varphi}_M\left[0.5(f_1+f_2)-\xi, -\lambda, 0.5(f_1+f_2)\right] \tilde{\mathbf{S}}(\xi,\lambda)\mathrm{d}\xi\mathrm{d}\lambda\\
&\overset{(a)}{=} \int_{-\infty}^{+\infty}\int_{-\infty}^{+\infty} F_\Pi\left[(f_2-f_1)-\lambda, 0.5(f_1+f_2)\right] \tilde{\varphi}_M\left[\xi-0.5(f_1+f_2), \lambda, 0.5(f_1+f_2)\right] \tilde{\mathbf{S}}(\xi,\lambda)\mathrm{d}\xi\mathrm{d}\lambda.
\end{aligned}
$$

where (a) is from the symmetric properties of $\varphi_M(f_1, f_2, f)$ indicated in Eq. (24). Eq. (38) can be proved from Eq. (86).

From Eq. (85), it can be obtained

$$
\begin{aligned}
&\hat{S}_{ij}^{*}(f_1, f_2)\hat{S}_{ij}(f_1, f_2)\\
&\quad=\int_{-\infty}^{+\infty}\int_{-\infty}^{+\infty}\Big\{F_{\Pi}^{*}\left[(f_2-f_1)-(\xi_2-\xi_1),0.5(f_1+f_2)\right]\\
&\qquad\qquad\times\varphi_M^{*}\left[0.5(f_1+f_2)-\xi_1,0.5(f_1+f_2)-\xi_2,0.5(f_1+f_2)\right]\Big\}\mathrm{d}Z_i(\xi_1)\mathrm{d}Z_j^{*}(\xi_2)\\
&\qquad\times\int_{-\infty}^{+\infty}\int_{-\infty}^{+\infty}\Big\{F_{\Pi}\left[(f_2-f_1)-(\lambda_2-\lambda_1),0.5(f_1+f_2)\right]\\
&\qquad\qquad\times\varphi_M\left[0.5(f_1+f_2)-\lambda_1,0.5(f_1+f_2)-\lambda_2,0.5(f_1+f_2)\right]\Big\}\mathrm{d}Z_i^{*}(\lambda_1)\mathrm{d}Z_j(\lambda_2)\\
&\quad=\int_{-\infty}^{+\infty}\int_{-\infty}^{+\infty}\int_{-\infty}^{+\infty}\int_{-\infty}^{+\infty}\Big\{F_{\Pi}^{*}\left[(f_2-f_1)-(\xi_2-\xi_1),0.5(f_1+f_2)\right]F_{\Pi}\left[(f_2-f_1)-(\lambda_2-\lambda_1),0.5(f_1+f_2)\right]\\
&\qquad\times\varphi_M^{*}\left[0.5(f_1+f_2)-\xi_1,0.5(f_1+f_2)-\xi_2,0.5(f_1+f_2)\right]\\
&\qquad\times\varphi_M\left[0.5(f_1+f_2)-\lambda_1,0.5(f_1+f_2)-\lambda_2,0.5(f_1+f_2)\right]\mathrm{d}Z_i(\xi_1)\mathrm{d}Z_j^{*}(\xi_2)\mathrm{d}Z_i^{*}(\lambda_1)\mathrm{d}Z_j(\lambda_2)\Big\}.
\end{aligned}
\tag{87}
$$

Then, the variance $\mathrm{Var}[\hat{S}_{ij}(f_1,\ f_2)]$ of $\hat{S}_{ij}(f_1,\ f_2)$ can be calculated as

$$
\begin{aligned}
&\mathrm{Var}\left[\hat{S}_{ij}(f_1, f_2)\right]\\
&\quad=\int_{-\infty}^{+\infty}\int_{-\infty}^{+\infty}\int_{-\infty}^{+\infty}\int_{-\infty}^{+\infty}\Big\{F_{\Pi}^{*}\left[(f_2-f_1)-(\xi_2-\xi_1),0.5(f_1+f_2)\right]F_{\Pi}\left[(f_2-f_1)-(\lambda_2-\lambda_1),0.5(f_1+f_2)\right]\\
&\quad\times\varphi_M^{*}\left[0.5(f_1+f_2)-\xi_1,0.5(f_1+f_2)-\xi_2,0.5(f_1+f_2)\right]\\
&\quad\times\varphi_M\left[0.5(f_1+f_2)-\lambda_1,0.5(f_1+f_2)-\lambda_2,0.5(f_1+f_2)\right]\mathrm{Cov}\left[\mathrm{d}Z_i(\xi_1)\mathrm{d}Z_j^{*}(\xi_2),\mathrm{d}Z_i^{*}(\lambda_1)\mathrm{d}Z_j(\lambda_2)\right]\Big\}.
\end{aligned}
\tag{88}
$$

Under the Gaussianity assumption on $\mathbf{X}(t)$, the complex version of the Isserlis' theorem [55, 56] expresses $\mathrm{Cov}[\mathrm{d}Z_i(\xi_1)\mathrm{d}Z_j^{*}(\xi_2),\ \mathrm{d}Z_i^{*}(\lambda_1)\mathrm{d}Z_j(\lambda_2)]$ as

$$
\begin{aligned}
&\mathrm{Cov}\left[\mathrm{d}Z_i(\xi_1)\mathrm{d}Z_j^{*}(\xi_2),\mathrm{d}Z_i^{*}(\lambda_1)\mathrm{d}Z_j(\lambda_2)\right]\\
&\quad=\mathrm{E}\left[\mathrm{d}Z_i(\xi_1)\mathrm{d}Z_i^{*}(\lambda_1)\right]\mathrm{E}\left[\mathrm{d}Z_j^{*}(\xi_2)\mathrm{d}Z_j(\lambda_2)\right]+\mathrm{E}\left[\mathrm{d}Z_i(\xi_1)\mathrm{d}Z_j(\lambda_2)\right]\mathrm{E}\left[\mathrm{d}Z_j^{*}(\xi_2)\mathrm{d}Z_i^{*}(\lambda_1)\right]\\
&\quad=S_{ii}^{*}(\xi_1,\lambda_1)S_{jj}(\xi_2,\lambda_2)\mathrm{d}\xi_1\mathrm{d}\lambda_1\mathrm{d}\xi_2\mathrm{d}\lambda_2+\mathrm{E}\left[\mathrm{d}Z_i(\xi_1)\mathrm{d}Z_j^{*}(-\lambda_2)\right]\mathrm{E}\left[\mathrm{d}Z_j^{*}(\xi_2)\mathrm{d}Z_i(-\lambda_1)\right]\\
&\quad=S_{ii}^{*}(\xi_1,\lambda_1)S_{jj}(\xi_2,\lambda_2)\mathrm{d}\xi_1\mathrm{d}\lambda_1\mathrm{d}\xi_2\mathrm{d}\lambda_2+S_{ij}^{*}(\xi_1,-\lambda_2)S_{ji}(\xi_2,-\lambda_1)\mathrm{d}\xi_1\mathrm{d}\lambda_2\mathrm{d}\xi_2\mathrm{d}\lambda_1.
\end{aligned}
\tag{89}
$$

Substituting Eq. (89) into Eq. (88), $\mathrm{Var}[\hat{S}_{ij}(f_1,\ f_2)]$ can be calculated as

$$
\mathrm{Var}\left[\hat{S}_{ij}(f_1, f_2)\right]=V_1(f_1, f_2)+V_2(f_1, f_2),
\tag{90}
$$

where

$$
\begin{aligned}
&V_1(f_1, f_2)\\
&\quad=\int_{-\infty}^{+\infty}\int_{-\infty}^{+\infty}\int_{-\infty}^{+\infty}\int_{-\infty}^{+\infty}\Big\{F_{\Pi}^{*}\left[(f_2-f_1)-(\xi_2-\xi_1),0.5(f_1+f_2)\right]F_{\Pi}\left[(f_2-f_1)-(\lambda_2-\lambda_1),0.5(f_1+f_2)\right]\\
&\quad\times\varphi_M^{*}\left[0.5(f_1+f_2)-\xi_1,0.5(f_1+f_2)-\xi_2,0.5(f_1+f_2)\right]\\
&\quad\times\varphi_M\left[0.5(f_1+f_2)-\lambda_1,0.5(f_1+f_2)-\lambda_2,0.5(f_1+f_2)\right]S_{ii}^{*}(\xi_1,\lambda_1)S_{jj}(\xi_2,\lambda_2)\Big\}\mathrm{d}\xi_1\mathrm{d}\lambda_1\mathrm{d}\xi_2\mathrm{d}\lambda_2
\end{aligned}
\tag{91}
$$

and

$$
\begin{aligned}
&V_2(f_1, f_2) \\
&= \int_{-\infty}^{+\infty}\int_{-\infty}^{+\infty}\int_{-\infty}^{+\infty}\int_{-\infty}^{+\infty}\left\{F_\Pi^*\left[(f_2-f_1)-(\xi_2-\xi_1), 0.5(f_1+f_2)\right]F_\Pi\left[(f_2-f_1)-(\lambda_2-\lambda_1), 0.5(f_1+f_2)\right]\right. \\
&\quad\times\varphi_M^*\left[0.5(f_1+f_2)-\xi_1, 0.5(f_1+f_2)-\xi_2, 0.5(f_1+f_2)\right] \\
&\quad\left.\times\varphi_M\left[0.5(f_1+f_2)-\lambda_1, 0.5(f_1+f_2)-\lambda_2, 0.5(f_1+f_2)\right]S_{ij}^*(\xi_1,-\lambda_2)S_{ji}(\xi_2,-\lambda_1)\right\}\mathrm{d}\xi_1\mathrm{d}\lambda_2\mathrm{d}\xi_2\mathrm{d}\lambda_1.
\end{aligned}
\tag{92}
$$

Further, $V_1(f_1, f_2)$ is approximated as

$$
\begin{aligned}
&V_1(f_1, f_2) \\
&= \int_{-\infty}^{+\infty}\int_{-\infty}^{+\infty}\int_{-\infty}^{+\infty}\int_{-\infty}^{+\infty}F_\Pi^*\left[(f_2-f_1)-(\lambda_1-\xi_1), 0.5(f_1+f_2)\right]F_\Pi\left[(f_2-f_1)-(\lambda_2-\xi_2), 0.5(f_1+f_2)\right] \\
&\quad\times\varphi_M^*\left[\xi_1-0.5(f_1+f_2), \lambda_1-0.5(f_1+f_2), 0.5(f_1+f_2)\right] \\
&\quad\times\varphi_M\left[\xi_2-0.5(f_1+f_2), \lambda_2-0.5(f_1+f_2), 0.5(f_1+f_2)\right]S_{ii}^*(\xi_1,\xi_2)S_{jj}(\lambda_1,\lambda_2)\mathrm{d}\xi_1\mathrm{d}\xi_2\mathrm{d}\lambda_1\mathrm{d}\lambda_2 \\
&= \int_{-\infty}^{+\infty}\int_{-\infty}^{+\infty}\int_{-\infty}^{+\infty}\int_{-\infty}^{+\infty}F_\Pi^*\left\{(f_2-f_1)-\left[\lambda-0.5\Delta\lambda-(\xi-0.5\Delta\xi)\right], 0.5(f_1+f_2)\right\} \\
&\quad\times F_\Pi\left\{(f_2-f_1)-\left[\lambda+0.5\Delta\lambda-(\xi+0.5\Delta\xi)\right], 0.5(f_1+f_2)\right\} \\
&\quad\times\varphi_M^*\left[\xi-0.5\Delta\xi-0.5(f_1+f_2), \lambda-0.5\Delta\lambda-0.5(f_1+f_2), 0.5(f_1+f_2)\right] \\
&\quad\times\varphi_M\left[\xi+0.5\Delta\xi-0.5(f_1+f_2), \lambda+0.5\Delta\lambda-0.5(f_1+f_2), 0.5(f_1+f_2)\right] \\
&\quad\times\tilde{S}_{ii}^*(\xi,\Delta\xi)\tilde{S}_{jj}(\lambda,\Delta\lambda)\mathrm{d}\xi\mathrm{d}\Delta\xi\mathrm{d}\lambda\mathrm{d}\Delta\lambda \\
&\overset{(a)}{\approx} \int_{-\infty}^{+\infty}\int_{-\infty}^{+\infty}\int_{-\infty}^{+\infty}\int_{-\infty}^{+\infty}F_\Pi^*\left\{(f_2-f_1)-\left[\lambda-0.5\Delta\lambda-(\xi-0.5\Delta\xi)\right], 0.5(f_1+f_2)\right\} \\
&\quad\times F_\Pi\left\{(f_2-f_1)-\left[\lambda+0.5\Delta\lambda-(\xi+0.5\Delta\xi)\right], 0.5(f_1+f_2)\right\} \\
&\quad\times\varphi_M^*\left[\xi-0.5(f_1+f_2), \lambda-0.5(f_1+f_2), 0.5(f_1+f_2)\right] \\
&\quad\times\varphi_M\left[\xi-0.5(f_1+f_2), \lambda-0.5(f_1+f_2), 0.5(f_1+f_2)\right]\tilde{S}_{ii}^*(\xi,\Delta\xi)\tilde{S}_{jj}(\lambda,\Delta\lambda)\mathrm{d}\xi\mathrm{d}\Delta\xi\mathrm{d}\lambda\mathrm{d}\Delta\lambda \\
&\overset{(b)}{\approx} \int_{-\infty}^{+\infty}\int_{-\infty}^{+\infty}\left|\varphi_M\left[\xi,\lambda,0.5(f_1+f_2)\right]\right|^2 \\
&\quad\times\int_{-\infty}^{+\infty}\int_{-\infty}^{+\infty}\left(F_\Pi^*\left\{(f_2-f_1)-\left[\lambda-0.5\Delta\lambda-(\xi-0.5\Delta\xi)\right], 0.5(f_1+f_2)\right\}\right. \\
&\qquad\times F_\Pi\left\{(f_2-f_1)-\left[\lambda+0.5\Delta\lambda-(\xi+0.5\Delta\xi)\right], 0.5(f_1+f_2)\right\} \\
&\qquad\left.\times\tilde{S}_{ii}^*\left[0.5(f_1+f_2),\Delta\xi\right]\tilde{S}_{jj}\left[0.5(f_1+f_2),\Delta\lambda\right]\right)\mathrm{d}\Delta\xi\mathrm{d}\Delta\lambda\mathrm{d}\xi\mathrm{d}\lambda \\
&\approx \int_{-\infty}^{+\infty}\int_{-\infty}^{+\infty}\left|\varphi_M\left[\xi,\lambda,0.5(f_1+f_2)\right]\right|^2 \\
&\quad\times\int_{-\infty}^{+\infty}\int_{-\infty}^{+\infty}\left(F_\Pi^*\left\{(f_2-f_1)-\left[\lambda-\xi+0.5(\Delta\xi-\Delta\lambda)\right], 0.5(f_1+f_2)\right\}\right. \\
&\qquad\times F_\Pi\left\{(f_2-f_1)-\left[\lambda-\xi+0.5(\Delta\lambda-\Delta\xi)\right], 0.5(f_1+f_2)\right\} \\
&\qquad\left.\times\tilde{S}_{ii}^*\left[0.5(f_1+f_2),\Delta\xi\right]\tilde{S}_{jj}\left[0.5(f_1+f_2),\Delta\lambda\right]\right)\mathrm{d}\Delta\xi\mathrm{d}\Delta\lambda\mathrm{d}\xi\mathrm{d}\lambda,
\end{aligned}
\tag{93}
$$

where (a) is from the assumption that the widths of $\varphi_M(\Delta\xi, \Delta\lambda)$ with respect to $\Delta\xi$ and $\Delta\lambda$ are wider than those of $\tilde{S}_{ii}(\xi, \Delta\xi)$ and $\tilde{S}_{jj}(\lambda, \Delta\lambda)$, respectively, and (*b*) is from the assumption that $\varphi_M(f_1, f_2)$ along the diagonal line $f_1 = f_2$ is narrower than that of $\mathbf{S}(f_1, f_2)$.

$V_2(f_1, f_2)$ is calculated as

$$
\begin{aligned}
&V_2(f_1, f_2)\\
&= \int_{-\infty}^{+\infty}\int_{-\infty}^{+\infty}\int_{-\infty}^{+\infty}\int_{-\infty}^{+\infty} \Big\{ F_\Pi^*\left[(f_2 - f_1) - (\xi_2 - \xi_1), 0.5(f_1 + f_2)\right] F_\Pi\left[(f_2 - f_1) - (\lambda_1 - \lambda_2), 0.5(f_1 + f_2)\right]\\
&\quad \times \varphi_M^*\left[0.5(f_1 + f_2) - \xi_1, 0.5(f_1 + f_2) - \xi_2, 0.5(f_1 + f_2)\right]\\
&\quad \times \varphi_M\left[0.5(f_1 + f_2) + \lambda_1, 0.5(f_1 + f_2) + \lambda_2, 0.5(f_1 + f_2)\right] S_{ij}^*(\xi_1, \lambda_2) S_{ji}(\xi_2, \lambda_1) \Big\} \mathrm{d}\xi_1 \mathrm{d}\lambda_2 \mathrm{d}\xi_2 \mathrm{d}\lambda_1\\
&= \int_{-\infty}^{+\infty}\int_{-\infty}^{+\infty}\int_{-\infty}^{+\infty}\int_{-\infty}^{+\infty} \Big\{ F_\Pi^*\left[(f_2 - f_1) - (\xi_2 - \xi_1), 0.5(f_1 + f_2)\right] F_\Pi\left[(f_2 - f_1) - (\lambda_1 - \lambda_2), 0.5(f_1 + f_2)\right]\\
&\quad \times \varphi_M^*\left[\xi_1 - 0.5(f_1 + f_2), \xi_2 - 0.5(f_1 + f_2), 0.5(f_1 + f_2)\right]\\
&\quad \times \varphi_M\left[\lambda_2 + 0.5(f_1 + f_2), \lambda_1 + 0.5(f_1 + f_2), 0.5(f_1 + f_2)\right] S_{ij}^*(\xi_1, \lambda_2) S_{ji}(\xi_2, \lambda_1) \Big\} \mathrm{d}\xi_1 \mathrm{d}\lambda_2 \mathrm{d}\xi_2 \mathrm{d}\lambda_1\\
&= \int_{-\infty}^{+\infty}\int_{-\infty}^{+\infty}\int_{-\infty}^{+\infty}\int_{-\infty}^{+\infty} F_\Pi^*\left[(f_2 - f_1) - (\lambda_2 - \xi_1), 0.5(f_1 + f_2)\right] F_\Pi\left[(f_2 - f_1) - (\lambda_1 - \xi_2), 0.5(f_1 + f_2)\right]\\
&\quad \times \varphi_M^*\left[\xi_1 - 0.5(f_1 + f_2), \lambda_2 - 0.5(f_1 + f_2), 0.5(f_1 + f_2)\right]\\
&\quad \times \varphi_M\left[\xi_2 + 0.5(f_1 + f_2), \lambda_1 + 0.5(f_1 + f_2), 0.5(f_1 + f_2)\right] S_{ij}^*(\xi_1, \xi_2) S_{ji}(\lambda_2, \lambda_1) \mathrm{d}\xi_1 \mathrm{d}\xi_2 \mathrm{d}\lambda_1 \mathrm{d}\lambda_2\\
&= \int_{-\infty}^{+\infty}\int_{-\infty}^{+\infty}\int_{-\infty}^{+\infty}\int_{-\infty}^{+\infty} F_\Pi^*\left[(f_2 - f_1) - (\lambda - 0.5\Delta\lambda - \xi + 0.5\Delta\xi), 0.5(f_1 + f_2)\right]\\
&\quad \times F_\Pi\left[(f_2 - f_1) - (\lambda + 0.5\Delta\lambda - \xi - 0.5\Delta\xi), 0.5(f_1 + f_2)\right]\\
&\quad \times \varphi_M^*\left[\xi - 0.5\Delta\xi - 0.5(f_1 + f_2), \lambda - 0.5\Delta\lambda - 0.5(f_1 + f_2), 0.5(f_1 + f_2)\right]\\
&\quad \times \varphi_M\left[\xi + 0.5\Delta\xi + 0.5(f_1 + f_2), \lambda + 0.5\Delta\lambda + 0.5(f_1 + f_2), 0.5(f_1 + f_2)\right]\\
&\quad \times \tilde{S}_{ij}^*(\xi, \Delta\xi) \tilde{S}_{ji}(\lambda, \Delta\lambda) \mathrm{d}\xi \mathrm{d}\Delta\xi \mathrm{d}\lambda \mathrm{d}\Delta\lambda\\
&\overset{(a)}{\approx} \int_{-\infty}^{+\infty}\int_{-\infty}^{+\infty}\int_{-\infty}^{+\infty}\int_{-\infty}^{+\infty} F_\Pi^*\left[(f_2 - f_1) - (\lambda - 0.5\Delta\lambda - \xi + 0.5\Delta\xi), 0.5(f_1 + f_2)\right]\\
&\quad \times F_\Pi\left[(f_2 - f_1) - (\lambda + 0.5\Delta\lambda - \xi - 0.5\Delta\xi), 0.5(f_1 + f_2)\right]\\
&\quad \times \varphi_M^*\left[\xi - 0.5(f_1 + f_2), \lambda - 0.5(f_1 + f_2), 0.5(f_1 + f_2)\right]\\
&\quad \times \varphi_M\left[\xi + 0.5(f_1 + f_2), \lambda + 0.5(f_1 + f_2), 0.5(f_1 + f_2)\right]\\
&\quad \times \tilde{S}_{ij}^*(\xi, \Delta\xi) \tilde{S}_{ji}(\lambda, \Delta\lambda) \mathrm{d}\xi \mathrm{d}\Delta\xi \mathrm{d}\lambda \mathrm{d}\Delta\lambda\\
&\approx \int_{-\infty}^{+\infty}\int_{-\infty}^{+\infty} \varphi_M^*\left[\xi - 0.5(f_1 + f_2), \lambda - 0.5(f_1 + f_2), 0.5(f_1 + f_2)\right]\\
&\quad \times \varphi_M\left[\xi + 0.5(f_1 + f_2), \lambda + 0.5(f_1 + f_2), 0.5(f_1 + f_2)\right]\\
&\quad \times \Big\{ \int_{-\infty}^{+\infty}\int_{-\infty}^{+\infty} F_\Pi^*\left[(f_2 - f_1) - (\lambda - \xi) + 0.5(\Delta\lambda - \Delta\xi), 0.5(f_1 + f_2)\right]\\
&\qquad \times F_\Pi\left[(f_2 - f_1) - (\lambda - \xi) - 0.5(\Delta\lambda - \Delta\xi), 0.5(f_1 + f_2)\right]\\
&\qquad \times \tilde{S}_{ij}^*(\xi, \Delta\xi) \tilde{S}_{ji}(\lambda, \Delta\lambda) \mathrm{d}\Delta\xi \mathrm{d}\Delta\lambda \Big\} \mathrm{d}\xi \mathrm{d}\lambda,
\end{aligned}
\tag{94}
$$

where (a) is from the assumption that the widths of $\varphi_M(\Delta\xi, \Delta\lambda)$ with respect to $\Delta\xi$ and $\Delta\lambda$ are wider than those of $\tilde{S}^*_{ij}(\xi, \Delta\xi)$ and $\tilde{S}_{ji}(\lambda, \Delta\lambda)$, respectively. Substituting Eqs. (93) and (94) into Eq. (90), Eqs. (41) to (44) are proved.

Appendix D. The proof of Theorem 3

Assuming that the time of stationarity of $\mathbf{X}(t)$ is larger than the width of the utilized windows $\psi_m(t, f)$, $m = 0, 1,\ldots, M-1$, at each time instant t, $\psi_m(k\Delta t - t, f)\mathbf{X}(k\Delta t)$ can be approximated as

$$\psi_m(k\Delta t - t, f)\mathbf{X}(k\Delta t) \approx \psi_m(k\Delta t, f)\mathbf{Y}_t(k\Delta t), \tag{95}$$

where $\mathbf{Y}_t(\tau)$ is a stationary process approximately representing the spectral properties of $\mathbf{X}(t)$ near t. The PSD matrix $\mathbf{P}_t(f)$ of $\mathbf{Y}_t(\tau)$ is formed by

$$P_{ij,t}(f) = W_{ij}(t, f), \tag{96}$$

where $P_{ij,\,t}(f)$ is the ij^{th} element of $\mathbf{P}_t(f)$. In this way, the estimators $\widehat{\mathbf{W}}(t, f)$ in Eq. (29) and $\widehat{C}_{ij}(t, f)$ in Eq. (32) can be respectively regarded as the multi-taper estimators for the PSD and coherence of $\mathbf{Y}_t(\tau)$. Under the assumption that $\widehat{\mathbf{W}}(t, f)$ is approximately unbiased, following the Theorem 2 and Appendix B in [44], Eqs. (45)-(50) can be directly obtained.

Appendix E. The proof of Theorem 4

Since the estimator $\hat{\hat{C}}_{ij}(f)$ in Eq. (34) is calculated by averaging $\widehat{C}_{ij}(t, f)$ in Eq. (32), the bias of $\hat{\hat{C}}_{ij}(f)$ can be directly obtained by replacing $C_{ij}(t, f)$ in Eq. (46) with $\overline{C}_{ij}(f)$, as indicated in Eqs. (51) and (52).

Under the condition that $C_{ij}(t, f)$ is time-invariant, as indicated in Eq. (33), the variance of $\widehat{C}_{ij}(t, f)$ can be calculated by replacing $C_{ij}(t, f)$ and $G_{ij}(t, f)$ in Eq. (50) with $\overline{C}_{ij}(f)$ and $T_{ij}(f)$, respectively

$$\operatorname{Var}\left[\hat{C}_{ij}(t, f)\right] \approx \frac{1}{M}\left[1-\left|\overline{C}_{ij}(f)\right|^2\right]^M {}_3F_2\left[2, M, M; M+1, 1; \left|\overline{C}_{ij}(f)\right|^2\right] - \left|\overline{C}_{ij}(f)\right|^2 T_{ij}^2(f), \tag{97}$$

where $T_{ij}(f)$ is in Eq. (52). In this situation, $\operatorname{Var}[\widehat{C}_{ij}(t, f)]$ is independent of time. In fact, the probability distribution of a non-parametric coherence estimator by the Fourier transform is only dependent on the corresponding theoretical coherence but independent of the related spectra, see Appendix B in [44]. Thus, in the case of a time-invariant coherence, $\widehat{C}_{ij}(t, f)$ at different time instants has the same probability distribution even though with time-varying spectra, and $\widehat{\widehat{C}}_{ij}(f)$ is a result calculated by averaging multiple random variates with the same probability distribution. However, $\widehat{C}_{ij}(t_1, f)$ and $\widehat{C}_{ij}(t_2, f)$, $t_1 \neq t_2$, may be not independent with a small time interval $\Delta t = t_2 - t_1$. Thus, the variance of $\widehat{\widehat{C}}_{ij}(f)$ cannot be directly calculated by dividing the Var[$\widehat{C}_{ij}(t, f)$] in Eq. (97) by the $L(f)$ in Eq. (34).

$\widehat{C}_{ij}(t_1, f)$ and $\widehat{C}_{ij}(t_2, f)$ can be assumed to be independent if $\psi_{M-1}(t - t_1, f)$ and $\psi_{M-1}(t - t_2, f)$ are non-overlapping. The width of $\psi_{M-1}(t, f)$ in the time domain is $2L_{\mathrm{v}}(f)$, where $L_{\mathrm{v}}(f)$ is in Eq. (31). Thus, in this study, at each f, $\widehat{\widehat{C}}_{ij}(f)$ is assumed to be the result calculated by averaging $N_{\mathrm{eq}}(f)$ independent $\widehat{C}_{ij}(t, f)$, where $N_{\mathrm{eq}}(f) = L(f)/L_{\mathrm{v}}(f)$ may not be an integer. Under this assumption, the variance of $\widehat{\widehat{C}}_{ij}(f)$ can be approximated by dividing the Var[$\widehat{C}_{ij}(t, f)$] in Eq. (97) by the $N_{\mathrm{eq}}(f)$, as indicated in Eqs. (53) and (54).

References

[1] M.B. Priestley, Evolutionary spectra and non-stationary processes, Journal of the Royal Statistical Society: Series B (Methodological), 27 (1965) 204-229.

[2] M.B. Priestley, H. Tong, On the analysis of bivariate non-stationary processes, Journal of the Royal Statistical Society: Series B (Methodological), 35 (1973) 153-166.

[3] G. Deodatis, Non-stationary stochastic vector processes: Seismic ground motion applications, Probabilistic Engineering Mechanics, 11 (1996) 149-167.

[4] J. Chen, F. Kong, Y. Peng, A stochastic harmonic function representation for non-stationary stochastic processes, Mechanical Systems and Signal Processing, 96 (2017) 31-44.

[5] D. Wang, Z. Fan, S. Hao, D. Zhao, An evolutionary power spectrum model of fully nonstationary seismic ground motion, Soil Dynamics and Earthquake Engineering, 105 (2018) 1-10.

[6] G. Huang, H. Zheng, Y.-l. Xu, Y. Li, Spectrum models for nonstationary extreme winds, Journal of Structural Engineering (ASCE), 141 (2015) 04015010.

[7] A. Kareem, L. Hu, Y. Guo, D.-K. Kwon, Generalized wind loading chain: Time-frequency modeling framework for nonstationary wind effects on structures, Journal of Structural Engineering, 145 (2019) 04019092.

[8] L. Roncallo, G. Solari, An evolutionary power spectral density model of thunderstorm outflows consistent with real-scale time-history records, Journal of Wind Engineering and Industrial Aerodynamics, 203 (2020) 104204.
[9] Z. Huang, Y.-L. Xu, T. Tao, S. Zhan, Time-varying power spectra and coherences of non-stationary typhoon winds, Journal of Wind Engineering and Industrial Aerodynamics, 198 (2020) 104115.
[10] G. Muscolino, T. Alderucci, Closed-form solutions for the evolutionary frequency response function of linear systems subjected to separable or non-separable non-stationary stochastic excitations, Probabilistic Engineering Mechanics, 40 (2015) 75-89.
[11] T. Alderucci, G. Muscolino, Fully nonstationary analysis of linear structural systems subjected to multicorrelated stochastic excitations, ASCE-ASME Journal of Risk and Uncertainty in Engineering Systems, Part A: Civil Engineering, 2 (2016) C4015007.
[12] Y. Li, J.P. Conte, M. Barbato, Influence of time-varying frequency content in earthquake ground motions on seismic response of linear elastic systems, Earthquake Engineering & Structural Dynamics, 45 (2016) 1271-1291.
[13] T. Tao, Y.-L. Xu, Z. Huang, S. Zhan, H. Wang, Buffeting analysis of long-span bridges under typhoon winds with time-varying spectra and coherences, Journal of Structural Engineering (ASCE), 146 (2020) 04020255.
[14] R.S. Langley, On quasi-stationary approximations to non-stationary random vibration, Journal of Sound and Vibration, 113 (1987) 365-375.
[15] F. Yamazaki, M. Shinozuka, Simulation of stochastic fields by statistical preconditioning, Journal of Engineering Mechanics, 116 (1990) 268-287.
[16] Z. Huang, Y.-L. Xu, S. Zhan, Conditionally simulating nonstationary typhoon winds with time-varying coherences for long-span bridges, Journal of Wind Engineering and Industrial Aerodynamics, 212 (2021) 104599.
[17] M. Loeve, Probability theory ii, Springer, 1978.
[18] M.M. Rao, The spectral domain of multivariate harmonizable processes, Proceedings of the National Academy of Sciences of the United States of America, 81 (1984) 4611-4612.
[19] A. Hanssen, Y. Larsen, L.L. Scharf, Complex time-frequency and dual-frequency spectra of harmonizable processes, 2004 12th European Signal Processing Conference, Vienna, Austria, 2004, pp. 1577-1580.
[20] P. Flandrin, Time-dependent spectra for non-stationary stochastic processes, Time and frequency representation of signals and systems, Springer, 1989, pp. 69-124.
[21] Z. Huang, Y. Xia, Probability distribution estimation for harmonisable loads and responses of linear elastic structures, Probabilistic Engineering Mechanics, 68 (2022) 103258.
[22] W. Martin, P. Flandrin, Wigner-ville spectral analysis of nonstationary processes, IEEE Transactions on Acoustics, Speech, and Signal Processing, 33 (1985) 1461-1470.
[23] F. Hlawatsch, F. Auger, Time-frequency analysis, John Wiley & Sons, 2013.
[24] W. Kozek, K. Riedel, Quadratic time-varying spectral estimation for underspread processes, Proceedings of IEEE-SP International Symposium on Time-Frequency and Time-Scale Analysis, IEEE, Philadelphia, PA, USA, 1994, pp. 460-463.
[25] A.M. Sayeed, D.L. Jones, Optimal kernels for nonstationary spectral estimation, IEEE Transactions on Signal Processing, 43 (1995) 478-491.
[26] M.G. Amin, Spectral decomposition of time-frequency distribution kernels, IEEE Transactions on Signal Processing, 42 (1994) 1156-1165.

[27] M. Bayram, R.G. Baraniuk, Multiple window time-varying spectrum estimation, in: W.J. Fitzgerald, R.L. Smith, A.T. Walden, P.C. Young (Eds.) Nonlinear and nonstationary signal processing, Cambridge University Press, Cambridge, U.K., 2000, pp. 292-316.

[28] Y. Wang, Time–frequency domain local spectral analysis of seismic signals with multiple windows, Proceedings of the Royal Society A, 478 (2022) 20220251.

[29] L.L. Scharf, B. Friedlander, Toeplitz and hankel kernels for estimating time-varying spectra of discrete-time random processes, IEEE Transactions on Signal Processing, 49 (2001) 179-189.

[30] J. Antoni, Cyclic spectral analysis in practice, Mechanical Systems and Signal Processing, 21 (2007) 597-630.

[31] H.L. Hurd, Spectral coherence of nonstationary and transient stochastic processes, Fourth Annual ASSP Workshop on Spectrum Estimation and Modeling, Minneapolis, MN, 1988, pp. 387-390.

[32] W. Gardner, Measurement of spectral correlation, IEEE Transactions on Acoustics, Speech, and Signal Processing, 34 (1986) 1111-1123.

[33] A. Napolitano, Uncertainty in measurements on spectrally correlated stochastic processes, IEEE Transactions on Information Theory, 49 (2003) 2172-2191.

[34] A. Napolitano, Cyclic statistic estimators with uncertain cycle frequencies, IEEE Transactions on Information Theory, 63 (2017) 649-675.

[35] D.J. Thomson, Spectrum estimation and harmonic analysis, Proceedings of the IEEE, 70 (1982) 1055-1096.

[36] D.J. Thomson, Multiple-window spectrum estimates for non-stationary data, Ninth IEEE Signal Processing Workshop on Statistical Signal and Array Processing (Cat. No.98TH8381), Portland, OR, 1998, pp. 344-347.

[37] L.L. Scharf, B. Friedlander, D.J. Thomson, Covariant estimators of time-frequency descriptors for nonstationary random processes, Conference Record of Thirty-Second Asilomar Conference on Signals, Systems and Computers (Cat. No. 98CH36284), IEEE, Pacific Grove, CA, 1998, pp. 808-811.

[38] J. Antoni, Cyclostationarity by examples, Mechanical Systems and Signal Processing, 23 (2009) 987-1036.

[39] P. Borghesani, The envelope-based cyclic periodogram, Mechanical Systems and Signal Processing, 58-59 (2015) 245-270.

[40] J. Bertrand, P. Bertrand, A class of affine wigner functions with extended covariance properties, Journal of Mathematical Physics, 33 (1992) 2515-2527.

[41] O. Rioul, P. Flandrin, Time-scale energy distributions: A general class extending wavelet transforms, IEEE Transactions on Signal Processing, 40 (1992) 1746-1757.

[42] P. Goncalves, R.G. Baraniuk, Pseudo affine wigner distributions: Definition and kernel formulation, IEEE Transactions on Signal Processing, 46 (1998) 1505-1516.

[43] A. Chaudhuri, S. Chakraborty, Sensitivity evaluation in seismic reliability analysis of structures, Computer Methods in Applied Mechanics and Engineering, 193 (2004) 59-68.

[44] Z. Huang, Y.L. Xu, A multi-taper S-transform method for spectral estimation of stationary processes, IEEE Transactions on Signal Processing, 69 (2021) 1452-1467.

[45] Z. Huang, Y.-L. Xu, T. Tao, Multi-taper S-transform method for evolutionary spectrum estimation, Mechanical Systems and Signal Processing, 168 (2022) 108667.

[46] Y.-M. Zhang, Z. Huang, Y. Xia, An improved multi-taper S-transform method to estimate evolutionary spectrum and time-varying coherence of nonstationary processes, Mechanical Systems and Signal Processing, 198 (2023) 110386.

[47] A. Hanssen, L.L. Scharf, A theory of polyspectra for nonstationary stochastic processes, IEEE Transactions

on Signal Processing, 51 (2003) 1243-1252.
[48] W. Martin, Time-frequency analysis of random signals, ICASSP '82. IEEE International Conference on Acoustics, Speech, and Signal Processing, 1982, pp. 1325-1328.
[49] C.E. Shannon, Communication in the presence of noise, Proceedings of the IRE, 37 (1949) 10-21.
[50] P. Flandrin, On the positivity of the wigner-ville spectrum, Signal Processing, 11 (1986) 187-189.
[51] L.B. White, B. Boashash, Cross spectral analysis of nonstationary processes, IEEE Transactions on Information Theory, 36 (1990) 830-835.
[52] R.G. Stockwell, L. Mansinha, R.P. Lowe, Localization of the complex spectrum: The S transform, IEEE Transactions on Signal Processing, 44 (1996) 998-1001.
[53] Y.-M. Zhang, Z. Huang, Y. Xia, An adaptive multi-taper spectral estimation for stationary processes, Mechanical Systems and Signal Processing, 183 (2023) 109629.
[54] A. Sklar, Random variables, joint distribution functions, and copulas, Kybernetika, 9 (1973) (449)-460.
[55] L. Isserlis, On a formula for the product-moment coefficient of any order of a normal frequency distribution in any number of variables, Biometrika, 12 (1918) 134-139.
[56] A.T. Walden, A unified view of multitaper multivariate spectral estimation, Biometrika, 87 (2000) 767-788.